Geo-Marine Letters
https://doi.org/10.1007/s00367-021-00696-6

ORIGINAL

Biogeochemistry of surface sediments in mud volcanoes of the Gulf of Cádiz

Dolores Jiménez-López[1] · Ana Sierra[1] · Teodora Ortega[1] · Sandra Manzano-Medina[1] · M. Carmen Fernández-Puga[2] · Nieves López-González[3] · Juan-Tomás Vázquez[3] · Jesús Forja[1]

Received: 18 December 2020 / Accepted: 29 April 2021

Abstract

The shallowest sediment of three mud volcanoes (MVs) located in the middle slope of the Gulf of Cádiz, Anastasya, Pipoca and St. Petersburg, have been seasonally studied during June and December 2016. These structures are locally important contributors of many biogeochemical active substances to the water column, with a special attention in the emission of methane (CH_4). Along this study, the role of organic matter diagenesis and its contribution to the diffusive fluxes estimated in the sediment–water interface from the three MVs have been investigated mainly. For this, the first combined analyses of sediment properties (granulometry, porosity, density, organic carbon) and pore water chemistry (major elements, dissolved inorganic carbon (DIC), nutrients, CH_4 and nitrous oxide) have been carried out. Anastasya and St. Petersburg MVs presented similar behaviours, with a slight concentration variation for the chemical variables in the top layers of the sedimentary record followed by a more intense vertical variation in deeper layers. Anastasya MV showed some typical processes of these structures, such as the clay dehydration, the dissolution of halite and the precipitation of authigenic carbonates, which was also observed in St. Petersburg MV. Organic matter diagenesis clearly altered the biogeochemical profiles, except for Pipoca MV. Moreover, mud breccia with a mousse-like texture has been identified in the deepest levels of Anastasya and St. Petersburg MVs. Here, anaerobic oxidation of methane is linked to the decrease of SO_4^{2-} and the increases of CH_4 and DIC with the core depth. Changes across the sediment–water interface presented low diffusive fluxes in the three MVs due to the presence of other processes as the irrigation by benthic macrofauna, the action of bottom currents and/or the upward fluid migration. From the obtained results, we can conclude that Anastasya MV presents a certain venting activity at present.

Keywords Mud volcanoes · Sediment · Biogeochemical processes · Authigenic carbonates · Fluid migration · Gulf of Cádiz

Introduction

Mud volcanoes (MVs) are cone-shaped structures, situated worldwide in active and passive continental margins at the earth's terrestrial surface or at the seafloor (e.g. Milkov, 2000; Dimitrov, 2002; Kopf, 2002). They are constructed mainly of mud and sedimentary constituents by the release of deep underground high-pressure argillaceous material, water and/or gases that rise up from a pressurized deep source through structurally controlled conduits (Brown, 1990; Dimitrov, 2003; Vanneste et al., 2011; León et al., 2012). Their shapes and sizes depend on the degree of mobilization of the pore-fluid pressures, such as the viscosity of the outflowing mud and the character or frequency of their activity (Dimitrov, 2002). The total number of identified MVs remains uncertain, but it has increased greatly in the last two decades. There are known to be about 900 terrestrial

✉ Dolores Jiménez-López
dolores.jimenez@uca.es

[1] Departamento de Química-Física, INMAR, Facultad de Ciencias del Mar y Ambientales, Universidad de Cádiz, Campus Universitario Río San Pedro, 11510 Puerto Real, Cádiz, Spain

[2] Departamento de Ciencias de La Tierra, INMAR, Facultad de Ciencias del Mar y Ambientales, Universidad de Cádiz, Campus Universitario Río San Pedro, 11510 Puerto Real, Cádiz, Spain

[3] Instituto Español de Oceanografía, Centro Oceanográfico de Málaga, Puerto Pesquero s/n Fuengirola, 29640 Málaga, Spain

Published online: 16 June 2021

MVs along with a global estimation of marine MVs range from 800 to 100,000 (Dimitrov, 2003; Kopf, 2003; Milkov et al., 2003; Niemann 2020).

Submarine MVs are one of the most common seafloor structures on the upper and middle continental slope of the Gulf of Cádiz (GoC), extending from the shelf down to 4500 m deep (e.g. Pinheiro et al., 2003; Somoza et al., 2003; Medialdea et al., 2009; León et al., 2012; Hensen et al., 2015; Palomino et al., 2016). Due to that, in this region, all the geological processes needed for the development of the MVs occur (Medialdea et al., 2009, and references therein). Until date, up to 80 MVs have been confirmed in the GoC through the mud breccia sediments retrieved from seafloor structures identified in seismic profiles (Magalhaes et al., 2019), although this number continues increasing (Sánchez-Guillamón, 2019). The importance of these seafloor structures is related to the migration of fluids and chemical elements from deep to shallow sediments, reaching the water column in certain cases (e.g. Aloisi et al., 2004; Medialdea et al., 2009; Carvalho et al., 2018; Magalhaes et al., 2019). There is a special interest in the fluid of hydrocarbons and mostly in the dominant expulsion of methane (CH_4) (Judd and Hovland, 2007). CH_4 is an important greenhouse gas affecting global climate change as well as an important commercial energy resource (e.g. Judd et al., 2002; Haese et al., 2003; Milkov and Etiope, 2005; Vanneste et al., 2011); therefore, a lot of studies are based on quantifying the flux of CH_4 from MVs. Milkov et al. (2003) estimated that about 27 Tg CH_4 $year^{-1}$ may escape from deep-water MVs. Also, Wallmann et al. (2006) evaluated that this CH_4 emission into the ocean via fluid flow through submarine MVs excluding the contributions from gas ebullition (~ 0.32 Tg CH_4 $year^{-1}$) and mud extrusions (~ 2 Tg CH_4 $year^{-1}$) was about 1.6 Tg CH_4 $year^{-1}$. If this CH_4 emission is compared with the range estimated of the marine CH_4 flux to the atmosphere from all marine waters (8.3–45.9 Tg CH_4 $year^{-1}$) (Bakker et al., 2014), mud volcanism should be considered as an important natural source of atmospheric CH_4. In the GoC, Vanneste et al. (2011) estimated a mean value of CH_4 emission of 0.53×10^{-5} Tg CH_4 $year^{-1}$ considering that all submarine MVs in this area (i.e. > 30) had the same level of activity as Captain Arutyunov and Carlos Ribeiro MVs.

Other processes that could be related to these structures are the precipitation of authigenic minerals, such as carbonate minerals (Aloisi et al., 2002; Pierre et al., 2012; Pereira et al., 2018) and the clay mineral dehydration (i.e. smectite–illite transformation) (Brown et al., 2001; Dählmann and De Lange, 2003; Martos-Villa et al., 2020). These happen due to the geochemical interactions with the adjacent sediments and rocks of the upward fluid provided by the MVs, which may alter the chemistry of the pore water (Hensen et al., 2007). The precipitation of carbonate minerals is promoted when the pore-fluid alkalinity increases during the release of bicarbonate, as a product of the anaerobic oxidation of methane (AOM), and the decrease of SO_4^{2-} at the pore water near the seafloor by the fluid migration of CH_4 along conduits in the MVs (Ritger et al., 1987; Borowski et al., 1996; Vanneste et al., 2011; Carvalho et al., 2018). The transformation from smectite to illite usually happens at deeper layers of the sediment with high temperatures between 60 and 150 °C (Colten-Bradley, 1987; Srodon, 1999), generating the release of Na^+ and the removal of K^+ to produce illite (Hower et al., 1976). In addition, some studies based on isotope measurements have suggested that hydrocarbon gas fluids are predominantly of thermogenic origin (Mazurenko et al., 2002; Niemann et al. 2006; Hensen et al., 2007; Nuzzo et al., 2009; Nakada et al., 2011; Vanneste et al., 2011). Stadnitskaia et al. (2006) also proposed that these hydrocarbons are of biogenic origin, being the result from a shallow bacterial source, which may be influenced by the partial recycling of thermogenic CH_4 in shallow sediments by AOM-related methanogenic archaea (Nuzzo et al., 2008).

Furthermore, the processes of organic matter mineralization and nutrient recycling also take place inside the sediment distributed through a vertical sequence of diverse microbial mechanisms, which use different terminal electron acceptors as oxidants (Berner, 1980; Boudreau, 1997). The aerobic oxidation of the organic matter occurs in the surface zone of the sediment, and when the oxygen is consumed, the anaerobic remineralization takes place mainly by sulphate reduction and methanogenesis (Reeburgh, 2007; Burdige, 2011).

There are numerous published works focused on MVs in the GoC discovered on both the Moroccan and Iberian continental margins (e.g. Ivanov et al., 2000; Díaz-del-Río et al., 2003; Somoza et al., 2003; Medialdea et al., 2009; León et al., 2012; Rueda et al., 2012; Rodrigues et al., 2013; Palomino et al., 2016). They are focused on different studies related to these structures, such as the morphology and geometry of the edifices, the geochemistry and origin of the fluid, the emissions of this fluid and also the characterization of the benthic fauna associated with fluid migration and seepage. But there is a minor attention on the study of biogeochemical and geological processes in pore water of the mud breccia sediments. Thus, the main aim of this work is to study the processes caused by organic matter diagenesis in the first 50 cm below the seafloor in the three MVs of the GoC. This allows a first approximation of the diffusive fluxes of different chemical species across the surface sediment in these systems and their relationships with the activity of the MVs.

Regional setting

The GoC is located in the westernmost tectonic belt of the Alpine–Mediterranean compressional system (the Gibraltar Arc in the front of the Betic–Rif belt), formed as a response to the convergence movements of the main plates of Eurasia and Nubia and the collision of the Alboran crustal domain both with the southern Iberian and the northern African continental margins (Maldonado et al., 1999; Pinheiro et al., 2003; Medialdea et al., 2009; Vázquez et al., 2020). This region is characterized by the presence of several seafloor structures related to hydrocarbon-rich fluid venting, such as mud volcanoes, pockmarks, carbonate chimneys and crusts, mud mounds and diapiric ridges (e.g. Díaz-del-Río et al., 2003; Somoza et al., 2003; Medialdea et al., 2004; Fernández-Puga et al., 2007; Magalhaes et al., 2019). The MVs are one of the most common seafloor structures on the Iberian and Moroccan margins of the GoC, mainly occurring on the continental slope, over a large area extending from 200 to 4500 m depth (Sánchez-Guillamón, 2019), and involving cone-shaped MVs of 400 to 4800 m diameter resulting from episodic flows of mud breccia (León et al., 2012). Also, they are associated with the diapiric structures yielded during a compressional–transpressional tectonic regime between the convergent plates, since they are located along deep routed faults or at their intersections with strike-slip faults (Pinheiro et al., 2003; Medialdea et al., 2009; Terrinha et al., 2009; Rosas et al., 2012; Hensen et al., 2015). These MVs are also the principal pathway for dewatering deep-sourced fluids of the GoC, being the clay mineral transformation and dehydration processes at depths of about 5 km below the seafloor the major source of the seepage fluids (Hensen et al., 2007; Nuzzo et al., 2009; Schmidt et al., 2018; Scholz et al., 2009).

This work was carried out in the three MVs of the GoC, Anastasya (7.151 ºW, 36.522 ºN), Pipoca (7.203 ºW, 36.460 ºN) and St. Petersburg (7.038 ºW, 35.897 ºN) (Fig. 1) (Díaz-del-Río et al., 2014; Palomino et al., 2016). Anastasya MV is the shallowest volcano in the study area, with its summit at 457 m water depth, 2 km of diameter, a height of 98 m and a symmetric regular cone shape with slopes ranging from 0.3 to 23º. Pipoca MV exhibits an asymmetrical cone shape, with diameters ranging from 1.1 to 2.9 km, a height of 107 m and the summit occurring at 503 m of water depth; its flanks have slopes that range from 0.5 to 25º. St. Petersburg MV is

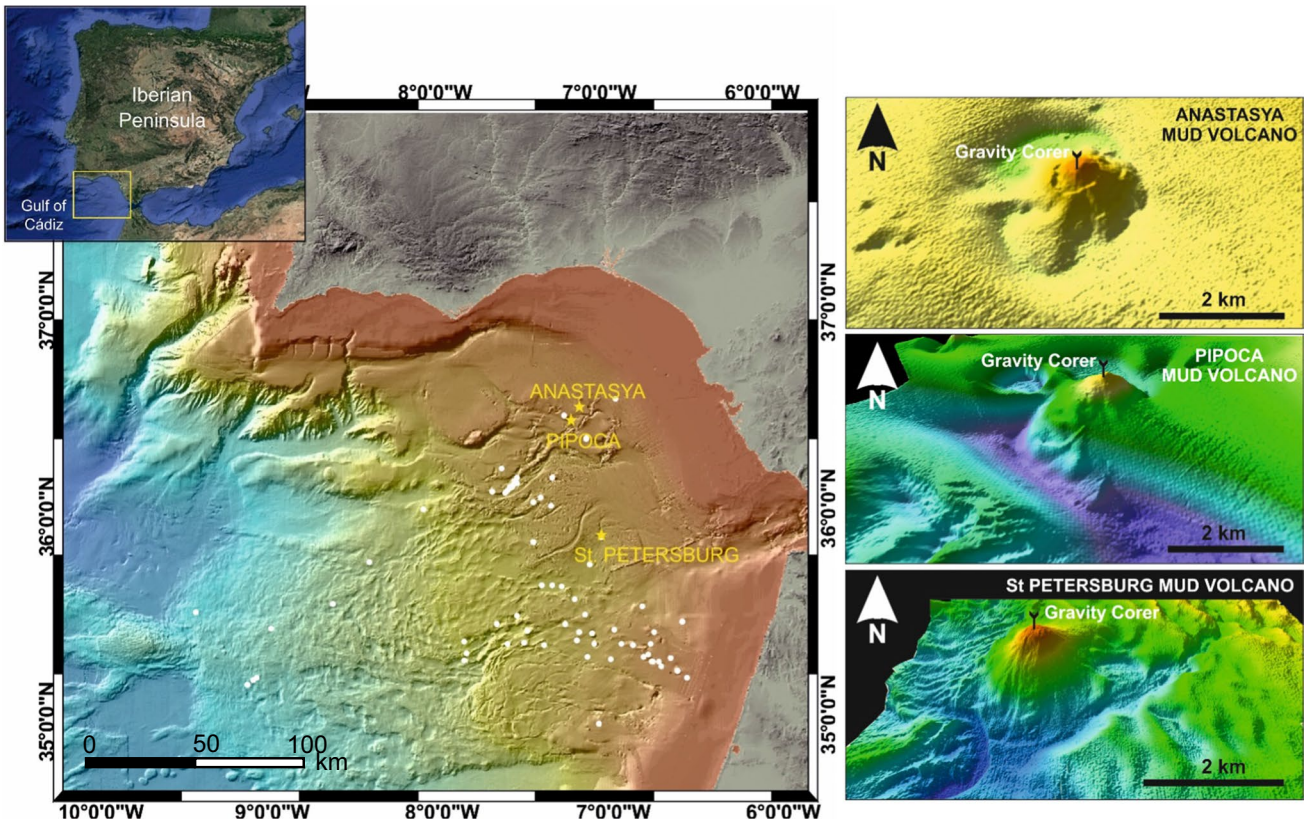

Fig. 1 Bathymetric map of the Gulf of Cádiz showing the location of the three sampled MVs (yellow stars): Anastasya, Pipoca and St. Petersburg MVs. The white dots indicate the position where other MVS are located on both the Moroccan and Iberian continental margins in the Gulf of Cádiz. Individual bathymetric maps of the three MVs studied are also shown on the right side of the main figure, together with the geographical positions of the cores

the deepest MV in this study, with an asymmetrical profile located between 935 and 1000 m water depth, a length of 2.1 km, a width of 1.8 km and a height of 132 m (Somoza et al., 2003; Fernández-Puga, 2004; Palomino et al., 2016).

Materials and methods

Sample collection

The samples were obtained during two cruises in June and December 2016, on board the R/V Ramón Margalef and Ángeles Alvariño, respectively, belonging to the Spanish Institute of Oceanography. Due to the bad weather conditions during December, St. Petersburg MV was not possible to sample. Three replicate gravity cores were taken for each MV and cruise, with a 1-m-long and 9.5 cm of inner diameter pipe. These cores were retrieved at the summit of the MVs (Fig. 1) since it is the area of preferably leaking of fluid and mud in recently active MVs (Palomino et al., 2016). Two of these cores were used for the determination of the biogeochemical and grain size variables and the third one for the quantification of CH_4 and nitrous oxide (N_2O) concentrations. All of the cores were carefully split in half lengthwise, photographed and described. For the analysis of biogeochemistry and granulometry, 1-cm-thick slices were subsampled at selected depths that depended on the core length as well as the observed textural changes observed just after opening. All sections were frozen (− 20 ºC) in N_2 atmosphere until their later treatment in the laboratory.

From the third core, duplicate samples for CH_4 and N_2O determinations were taken for each selected depth of the sediment with 5-mL cut-tip syringes and were then frozen (− 20 ºC) until their analysis in the laboratory. Moreover, the bottom water samples were taken from the positions belonging to each of the three MV studied with the use of Niskin bottles (10 L), which were mounted on a rosette sampler coupled to a Sea-Bird CTD 911 + .

Sample treatment and analytical methods

Subsamples for the determination of CH_4 and N_2O concentrations in the sediment were extracted from the syringes and weighed within septum vials of 23.9 mL, resulting between 2.64 and 4.65 g (± 0.01 g). The vials were filled with 5 mL of seawater previously fixed with mercuric chloride and saturated with a gas standard that had CH_4 and N_2O concentrations close to atmospheric values (1.8 ppmv of CH_4 and 0.3 ppmv of N_2O). Then, they were finally completed with air from the laboratory and vigorously shaken to equilibrate sediment–water–atmosphere phases. The air from the laboratory was also sampled regularly in order to correct the sediment concentrations. For the sediment samples, once equilibrium was reached, a 10-mL chromatography syringe was used to extract 5 mL of the headspace, operating at the same time with a second syringe that introduced a high-density solution (KCl 3 M) to maintain atmospheric pressure (Burgos et al., 2015). Equilibration temperature of the laboratory was measured, obtaining a range between 21.6 and 22.9 ºC (± 0.01 ºC).

Duplicated water samples for dissolved CH_4 and N_2O determinations in the bottom water were taken carefully in 250-mL airtight glass bottles, preserved with saturated mercuric chloride to inhibit microbial activity and sealed with Apiezon® grease to prevent gas exchange. A headspace was also created in a chromatographic glass syringe of 50 mL for CH_4 and N_2O measurements. Thus, 25 g (± 0.01 g) of water were taken, and the volume of the syringe was completed with the same standard gas used in the sediment. For each airtight glass bottle, this operation was repeated twice. The syringes were shaken vigorously for 5 min to ensure the equilibration (Sierra et al., 2017).

Subsequently, both sediment and water samples were measured using a gas chromatograph (Bruker® GC-450). The configuration of this instrument permits the simultaneous analysis of CH_4 and N_2O. It is necessary to calibrate the detectors daily, using four standard gas mixtures, which were made and certified by Abello Linde, with CH_4 and N_2O concentrations of 1.8, 3.0, 10.0 and 100.0 ppmv and 0.3, 0.4, 0.5 and 2.0 ppmv, respectively. Finally, the created headspaces were injected in the chromatograph to determine the concentrations of the gases, using the functions of solubility given by Wiesenburg and Guinasso (1979) for CH_4 and Weiss and Price (1980) for N_2O. The precision in the quantification of the gases was of 6.4% for CH_4 and 4.5% for N_2O in sediment samples and 1.7% for CH_4 and of 3.3% for N_2O in water samples.

The particle size distribution of the bulk sediment samples was carried out using a laser diffractometer (Malvern Mastersizer 3000), which measures particles in a range from 0.02 µm to 3 mm that comprise the proportion of sand, silt and clay. For organic matter oxidization, each sample was previously treated with hydrogen peroxide (10%) and dispersed by adding 1% solution of sodium hexametaphosphate to avoid flocculation. The measurements were conducted in liquid dispersion at between 10 and 20% obscuration range during 30 s under moderately high pump and stirrer settings (2500 rpm). Every result is the average of three successive laser diffraction runs.

For the determination of the other variables, for each slice, it was necessary to separate the sediment from the pore water. Therefore, the sections were previously unfrozen; about 100 g of sample in duplicate was homogenized and centrifuged (30 min, 10,000 g and 10 ºC, SIGMA-18KS). The sediment was then dried at 60 ºC until a constant weight was obtained, and then it was crushed with a planetary ball

mill (Retsch PM 200) and finally sieved (63 µm). The density of the sediment was quantified through Gay-Lussac pycnometer of 25 mL (Flint and Flint 2002), and the dried portions of sediment were analysed for carbon (C), nitrogen (N) and sulphur (S) with an elemental analyser (LECO CHNS932) (Grasshoff and Ehrhardt, 1983). Organic C (C_{org}) was determined after removing inorganic C by acidification, following the method described by Hedges and Stern (1984). Sediment porosity was determined from the weight of water loss after drying a pre-weighed amount of the wet sediment and considering the density of the dry sediment and the pore water (Boudreau, 1997).

Samples of pore water and bottom waters were filtered with glass filters (Millipore HPF 0.45 µm and Whatman GF/F 0.7 µm, respectively) before their analysis. pH and total alkalinity (TA) were measured in 2 mL and 100 mL of pore and bottom water, respectively. Both were performed by duplicate through potentiometric titration (Metrohm 905) with a glass-combined electrode calibrated in the total pH scale (Zeebe and Wolf-Gladrow, 2001). The TA measurements were validated with reference standards supported from A. Dickson (Scripps Institute of Oceanography, San Diego, USA, Batch # 153) with an accuracy of ± 0.012 mM and ± 0.003 mM for pore and bottom waters, respectively. Dissolved inorganic carbon (DIC) was calculated by means of the CO2SYS program (Lewis et al., 1998), including the K1 and K2 acidity constants proposed by Lueker et al. (2000) in the total pH scale, the HSO_4^- constant of Dickson (1990) and the total boron constant of Lee et al. (2010). The in situ conditions of temperature, salinity, pressure and PO_4^{3-} concentrations were also considered in this calculation. Moreover, pH values were also normalized at a temperature of 20 ºC (pH at 20 ºC) through this CO2SYS program in the same conditions described previously.

Cations (Na^+, K^+, Ca^{2+}, Mg^{2+}) and anions (Cl^- and SO_4^{2-}) were measured in the pore water by an ionic chromatograph (Metrohm 881/882, Compact IC pro, plus), with a variation coefficient in the analyses of 1.78 ± 0.26%. Concentrations in the bottom water were calculated from salinity, considering a conservative behaviour of the major ions in the seawater (Millero, 2013). By using the measured Cl^- values in the pore water of the MVs, a salinization ratio was calculated at each depth, expressed as a percentage of the pore water value and using the following equation (Kim et al. 2013):

$$\text{Salinization} = \left(\left(Cl^-_{pw} - Cl^-_{sw}\right)/Cl^-_{pw}\right) \cdot 100$$

where Cl^-_{pw} is the measured Cl^- value in the pore water and Cl^-_{sw} is the calculated Cl^- concentration in the bottom water for the different MVs.

Nutrients analysis, in both pore and bottom waters, was performed in a segmented flow auto-analyser (Skalar, San Plus) based on classic spectrophotometric methods (Grasshoff et al., 1983). The precision in the determination of PO_4^{3-}, NH_4^+, NO_3^- and NO_2^- was of ± 0.02 µM, ± 0.20 µM , ± 0.10 µM and ± 0.0.2 µM, respectively.

Calculation of fluxes

Diffusive fluxes across the sediment–water interface for some species were calculated using the Fick's first law of diffusion (Berner, 1980):

$$F = \phi D_s(\partial C/\partial Z)_{z=0}$$

where F is the diffusive flux, ϕ is the porosity of the surface sediment, D_s is the molecular diffusion coefficient in the sediment, and the term $(\partial C/\partial Z)_{z=0}$ is the result of the best linear relationship between the concentration of each specie and the existing concentration in the surface layer of the sediment (Table 1). A positive flux indicates that there is a transfer of solutes from the sediment to the water column. Furthermore, D_s has been corrected for porosity values following Boudreau (1997):

$$D_s = D^0/(1 + (n(1 - \phi)))$$

where D^0 is the diffusion coefficient to infinite dilution calculated at a given temperature with the expressions proposed by Broecker and Peng (1974) for CO_2, CH_4 and N_2O and Li and Gregory (1974) for PO_4^{3-}, NH_4^+, NO_3^-,NO_2^-, HCO_3^- and CO_3^{2-}. And the term n makes reference to the porosity of the sediment, with a value of 3 for clays and silt (Iversen and Jørgensen, 1993). The diffusive fluxes of DIC have been estimated from the sum of the fluxes of CO_2, HCO_3^- and CO_3^{2-} (Cai et al., 2000; Mucci et al., 2000) and the diffusive fluxes of TA from the sum of the fluxes of HCO_3^- and two times the fluxes of CO_3^{2-} (Ortega et al., 2008). Despite that the advection speed of the fluid in the sediment has been estimated, the diffusive fluxes calculated across the sediment–water interface will represent a first approximation, since the advective fluxes in the sediment were not considered.

The advection speed of the fluid has been estimated following the method proposed by Haese et al. (2003). It is based on the application of a 1D model of transport by diffusion and advection applicable to those solutes that present a conservative behaviour (Haese et al., 2003, 2006; Vanneste et al., 2011). Porosity and advection velocity are considered to remain constant with depth. Haese et al. (2003) present the integrated equation when the concentrations in the upper and lower boundaries are fixed, which allows establishing the theoretical variation of the solute concentration for different advection speeds. The range of variation of advection speeds has been obtained by comparing the experimental concentrations with those generated for the different advection speeds. With this advection

Table 1 Best linear relationships from the concentrations of PO_4^{3-}, NH_4^+, NO_3^-, NO_2^-, HCO_3^-, CO_3^{2-}, CO_2, CH_4 and N_2O in the surface zone of the sediment for the different MVs sampled (Anastasya, Pipoca and St. Petersburg) during the cruises of June and December

	Anastasya MV						Pipoca MV						St. Petersburg MV		
	June			December			June			December			June		
Specie	*n*	Equation	r^2	*n*	Equation	r^2	*n*	Equation	r^2	*n*	Equation	r^2	*n*	Equation	r^2
PO_4^{3-}	5	$C=0.134\,z+1.29$	0.63	6	$C=0.133\,z+1.03$	0.81	5	$C=0.224\,z+1.87$	0.57	6	$C=0.391\,z+2.29$	0.67	4	$C=0.267\,z+1.38$	0.90
NH_4^+	4	$C=9.308\,z+11.46$	0.80	4	$C=10.083\,z+10.83$	0.64	4	$C=3.311\,z+18.90$	0.55	4	$C=14.872\,z+12.40$	0.71	5	$C=4.356\,z+9.83$	0.90
NO_3^-	4	$C=-1.989\,z+8.73$	0.59	4	$C=-1.502\,z+9.23$	0.32	4	$C=-2.051\,z+9.47$	0.65	4	$C=-1.958\,z+6.31$	0.44	4	$C=-2.303\,z+13.32$	0.83
NO_2^-	4	$C=0.031\,z+0.10$	0.68	4	$C=0.013\,z+0.10$	0.35	4	$C=0.602\,z+0.81$	0.46	4	$C=0.054\,z+0.07$	0.52	3	$C=0.269\,z+1.44$	0.14
HCO_3^-	5	$C=34.557\,z+2028.4$	0.83	5	$C=89.387\,z+2255.5$	0.71	4	$C=20.633\,z+1709.5$	0.88	4	$C=187.147\,z+1763.8$	0.99	3	$C=-3.634\,z+1838.0$	0.27
CO_3^{2-}	4	$C=63.099\,z+176.8$	0.74	5	$C=5.247\,z+43.4$	0.76	3	$C=4.363\,z+187.5$	0.95	4	$C=8.670\,z+19.9$	0.81	3	$C=21.166\,z+183.8$	0.73
CO_2	4	$C=-1.369\,z+15.7$	0.64	4	$C=15.889\,z+45.7$	0.39	3	$C=0.434\,z+11.4$	0.70	3	$C=-14.982\,z+116.9$	0.77	4	$C=0.087\,z+8.5$	0.91
CH_4	4	$C=0.129\,z+0.33$	0.32	4	$C=0.099\,z+0.80$	0.36	5	$C=0.010\,z+0.02$	0.90	4	$C=0.028\,z+0.02$	0.77	3	$C=0.032\,z+0.05$	0.15
N_2O	4	$C=0.116\,z+0.19$	0.85	4	$C=0.105\,z+0.31$	0.53	4	$C=0.110\,z+0.21$	0.65	4	$C=0.166\,z+0.48$	0.49	4	$C=0.052\,z+0.01$	0.95

The number of data considered in the adjustment including the bottom water is shown (*n*), as well as the resulting equation used where *C* is the concentration of the specie (μM) and *z* the depth along the core (cm), including the correlation coefficients of the adjustment (r^2)

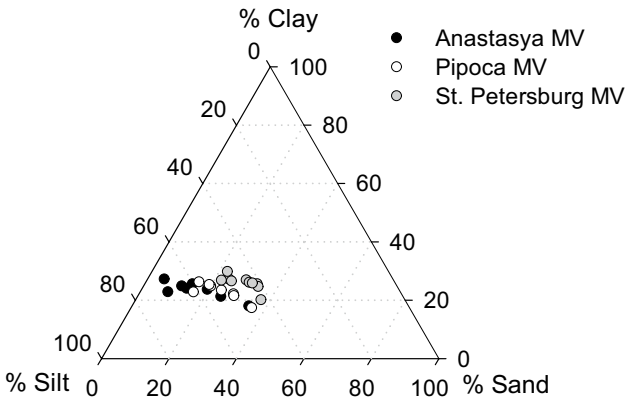

Fig. 2 Ternary diagram indicating the particle size percentage variation of the sediment samples analysed in the cores retrieved from the three MVs (Anastasya, Pipoca and St. Petersburg) during the oceanographic expedition in June

speed, it is possible to calculate the advective flux in the shallow layer of the sediment through the advection speed of the fluid and the concentration of the solute as Niemann (2020) described.

Statistical analysis

Statistical analyses were performed using IBM SPSS Statistics software (version 20.0; Armonk, NY, USA). The dataset was analysed using a one-way analysis of variance test (ANOVA) for analysing significant differences between MVs for the characteristics determined in the sediment and in the pore water. The threshold value for statistical significance was taken as $p < 0.05$.

Results

Sediment characterization

Sediment texture expressed in terms of percentage of sand, silt and clay does not show significant differences between all the MVs, except for the sand content. The highest percentage corresponded to silt in the three MVs (Fig. 2), with mean values ranging between 44.9 ± 3.6 and 60.0 ± 6.5 vol% (Table 2). The proportion of clay was relatively constant among the three MVs, with a mean value of 23.7 ± 3.3 vol%. As mentioned above, the percentages of sand were more variable between the MVs as well as along the core length, with values ranging between 5.1 and 46.2 vol%.

Figure 3 shows the sedimentary record for each MV, where only one sediment core log was selected as the most representative of the facies distribution for each MV and both cruises. The sediment recovered in Anastasya MV (48 cm length) is characterized by a thin veneer (0–8 cm) of olive grey (5Y 5/2, according to the Munsell Color Chart, 2000) (Table 2) hemipelagic sediment overlying a greenish-grey (GLEY1 5/5G) of mud breccia (8–20 cm). Some breccia clasts were observed at core depths between 8 and 20 cm, embedded in the mud breccia. From about 20 cm to the bottom of the core, a mousse-like texture was clearly observed due to the presence of methane-rich sediments. In Pipoca MV, the sediment core (50 cm length) displayed a quite homogeneous sedimentary column of greenish-grey (GLEY1 5/5G) mud breccia that is overlain by a thin layer of olive grey hemipelagic sediments (5Y 5/2). Interbedded hemipelagic sediments were observed at the top but could be a result of the core retrieval. Some breccia clasts were

Table 2 Mean values and standard deviations of the studied properties in the sediments of the three MVs studied, including density; porosity; median diameter of the particle (D50); volume percentage of clay, sand and silt; the content of carbon (C), nitrogen (N), sulphur (S) and organic carbon (C_{org}); and the sediment colour for different depths along the core length

	Anastasya MV	Pipoca MV	St. Petersburg MV
% clay	23.2 ± 2.9	22.0 ± 3.4	25.8 ± 2.5
% sand	16.8 ± 8.9	26.3 ± 9.5	29.2 ± 5.3
% silt	60.0 ± 6.5	51.7 ± 6.4	44.9 ± 3.6
Density (g mL^{-1})	2.54 ± 0.12	2.54 ± 0.04	2.54 ± 0.05
Porosity	0.59 ± 0.03	0.59 ± 0.02	0.55 ± 0.02
D50 (μm)	11.9 ± 3.7	16.6 ± 11.3	13.2 ± 4.0
C (%)	1.56 ± 0.16	1.80 ± 0.08	1.94 ± 0.06
N (%)	0.09 ± 0.01	0.10 ± 0.01	0.10 ± 0.01
S (%)	1.61 ± 0.35	0.73 ± 0.15	0.52 ± 0.08
C_{org} (%)	1.17 ± 0.12	1.34 ± 0.05	1.45 ± 0.06
Mean colour (≈ 1–3 cm)	Olive grey (5Y 5/2)	Olive grey (5Y 5/2)	Olive (5Y 5/3)
Mean colour (> 10 cm)	Greenish-grey (GLEY1 5/5G)	Greenish-grey (GLEY1 5/5G)	Greenish-grey (GLEY1 5/10Y)

The values are result of the obtained average from the complete cores' length for the two cruises (June and December) and the sediment colour was visually estimated using Munsell colour chart (2000)

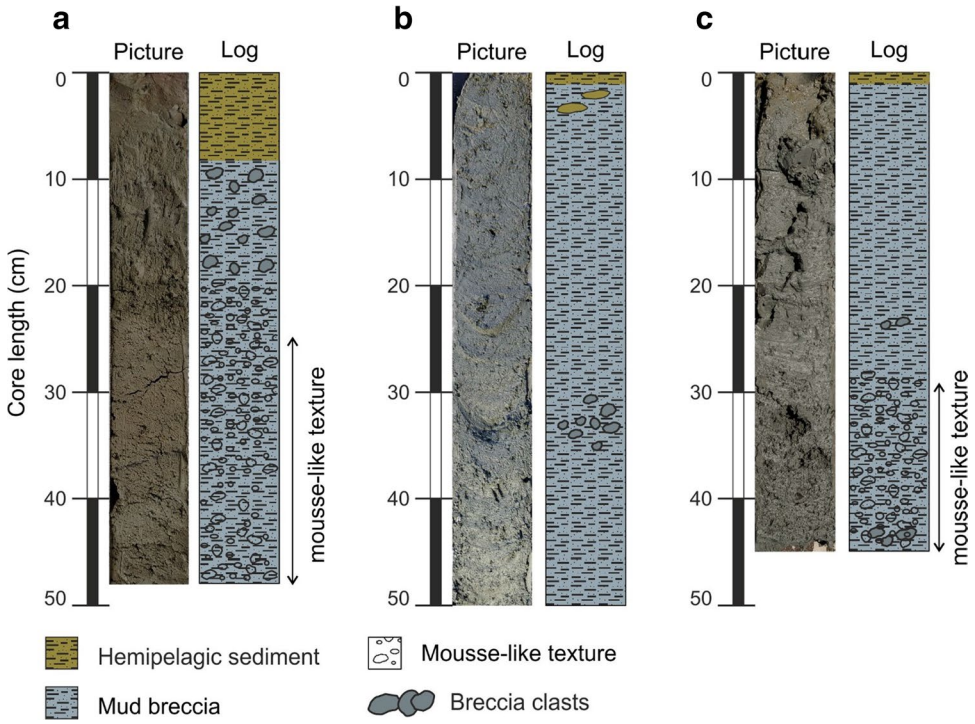

Fig. 3 Sediment core logs of the studied MVs: Anastasya (**a**), Pipoca (**b**) and St. Petersburg (**c**). The main sedimentary facies observed were hemipelagic sediments, at the top of all cores, and mud breccia of different texture

observed at core depths between 28 and 35 cm. And finally, in the case of St. Petersburg MV sediment core (45 cm length), a yielded greenish-grey (GLEY1 5/10Y) mud breccia texture that changed to a mousse-like texture from about 28 cm to the core base was observed. Some small breccia clasts were observed at ca. 25 cm deep and at the core bottom. The hemipelagic sediment of olive colour (5Y 5/3) was only present as a thin layer at the core top.

The vertical profiles for density, porosity and median diameter of the particle size (D50) in dry sediment are shown in Fig. 4. The density values had no significant differences among the MVs, with a similar mean value of 2.54 ± 0.08 g mL^{-1} (Table 2). Porosity presented significant differences between the MVs with a general tendency to decrease with depth in the different cores. The dominant sediment fraction for D50 in the three MVs was fine silt (over 80% of the total samples), with a mean value of 13.9 ± 7.3 µm, except for some levels characterized by medium and coarse silt (Fig. 4).

For the three MVs, the content of C, S and C_{org} in the sediment presented significant differences, but the values of N remained relatively constant along the profiles (0.09–0.11%) (Table 2). Pipoca and St. Petersburg MVs barely showed variations of these variables with depth (Fig. 5). However, C and C_{org} profiles throughout June for Anastasya MV presented more pronounced changes, with a relative decrease of 32.3% and 31.7% along the core, respectively. Additionally, in the case of Anastasya MV, an increase of S over 10 cm core deep in the first 10 cm in both cruises was observed, reaching values of 2%, and a noticeable H_2S smell was detected when opening the cores.

Major elements

Most of the major elements (Na^+, K^+, Ca^{2+} and Mg^{2+}) in the top first centimetres of the pore water were slightly enriched with respect to the bottom water (Fig. 6). In general, the vertical profiles of the major elements differed between the three MVs. Anastasya and St. Petersburg MVs presented a constant concentration in the sediment from the top, down to 15–20 cm and 28–30 cm core deep, respectively, as well as a vertical variation at those depths. The changes observed for Anastasya MV between cruises could be due to the spatial heterogeneity in the sampled sediment (Vanneste et al., 2011). However, Pipoca MV showed similar values along the cores for all elements, with small differences between the uppermost and bottom depths.

Na^+ and Cl^- concentrations increased with depth in Anastasya MV (Fig. 6), having a mean increase of 351.3 ± 64.9 and 256.5 ± 111.3 mM between the surface and bottom sediments of the core, respectively. Pipoca and St. Petersburg MV profiles remained practically constant with respect to the core depth and between cruises, with a sharp decrease of Na^+ at the bottom sediments of St. Petersburg MV. Although the mean values of Na^+ in Pipoca MV (530.1 ± 45.3 mM) were lower than those in St. Petersburg MV (570.5 ± 45.1 mM), Cl^- mean values were similar for both MVs (544.1 ± 25.5 and 546.9 ± 11.6 mM, respectively). Similarly, K^+, Ca^{2+},

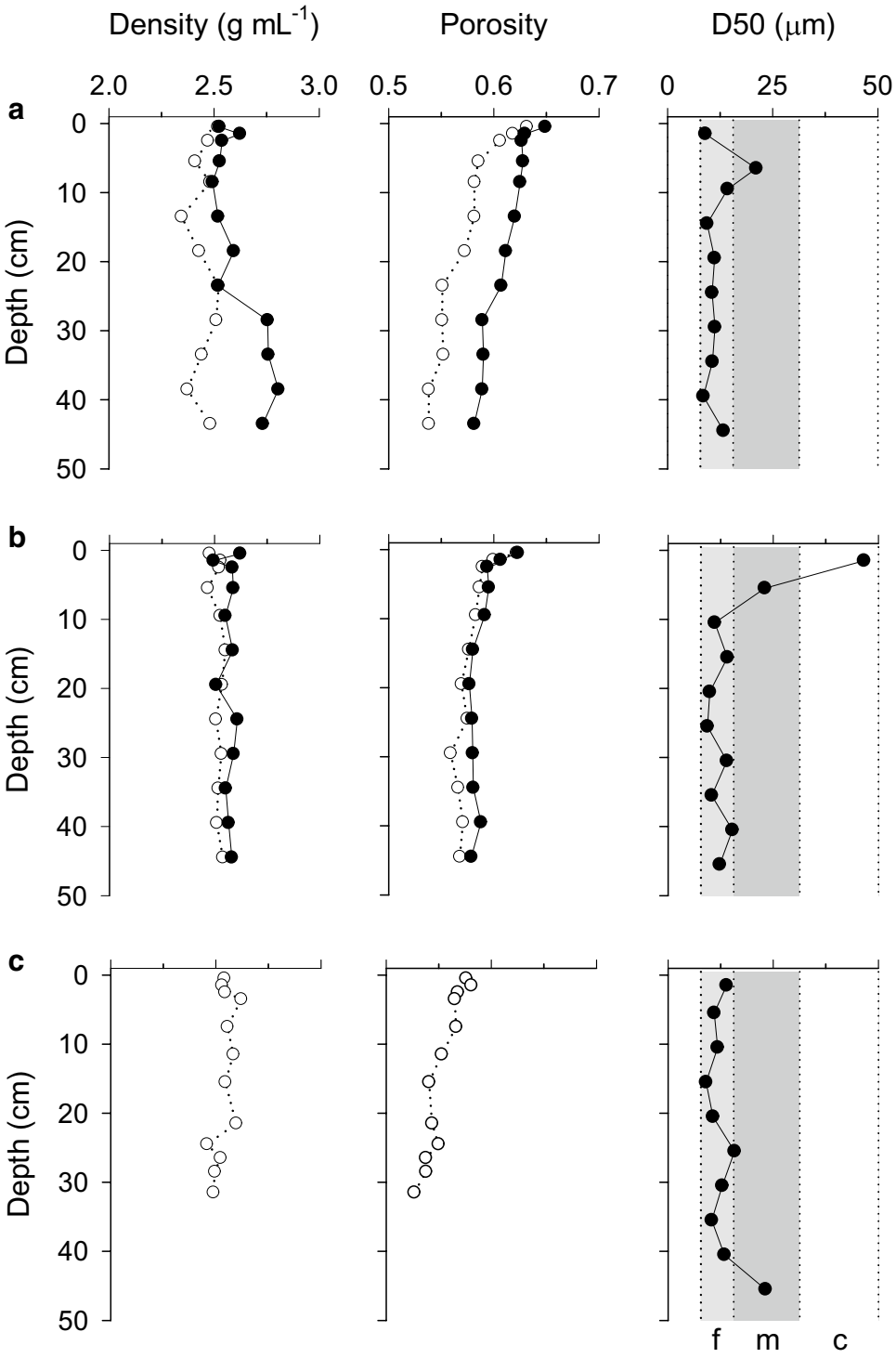

Fig. 4 Sediment profiles of density, porosity and median diameter of the particle size (D50) measured in sediment samples of cores retrieved in the cruises of June (white circles) and December (black circles) for the three MVs: Anastasya (**a**), Pipoca (**b**) and St. Petersburg (**c**). Shaded zones in D50 profiles correspond to different ranges of diameter for silt (fine (f), medium (m) and coarse (c)) according to Udden–Wentworth scheme (Udden, 1914; Wentworth, 1922)

Mg^{2+} and SO_4^{2-} concentrations tended to decrease with the core depth in the case of Anastasya and St. Petersburg MVs with a more pronounced reduction from 18.5 and 28.5 cm to the base, respectively. Except for Ca^{2+} throughout the December cruise in Anastasya MV, that remained relatively constant (Fig. 6). The highest average decrease of K^+, Ca^{2+}, Mg^{2+} and SO_4^{2-} with respect to the surface sediment resulted for Anastasya MV during both cruises (3.3 ± 1.6, 2.8 ± 0.2, 33.8 ± 1.4 and 24.0 ± 1.2 mM, respectively). On the other hand, the lowest average decrease values were generally observed in St. Petersburg MV (3.5, 6.2, 29.8 and 11.8 mM). However, Pipoca MV presented more constant profiles with concentration mean values similar to those obtained in the bottom water.

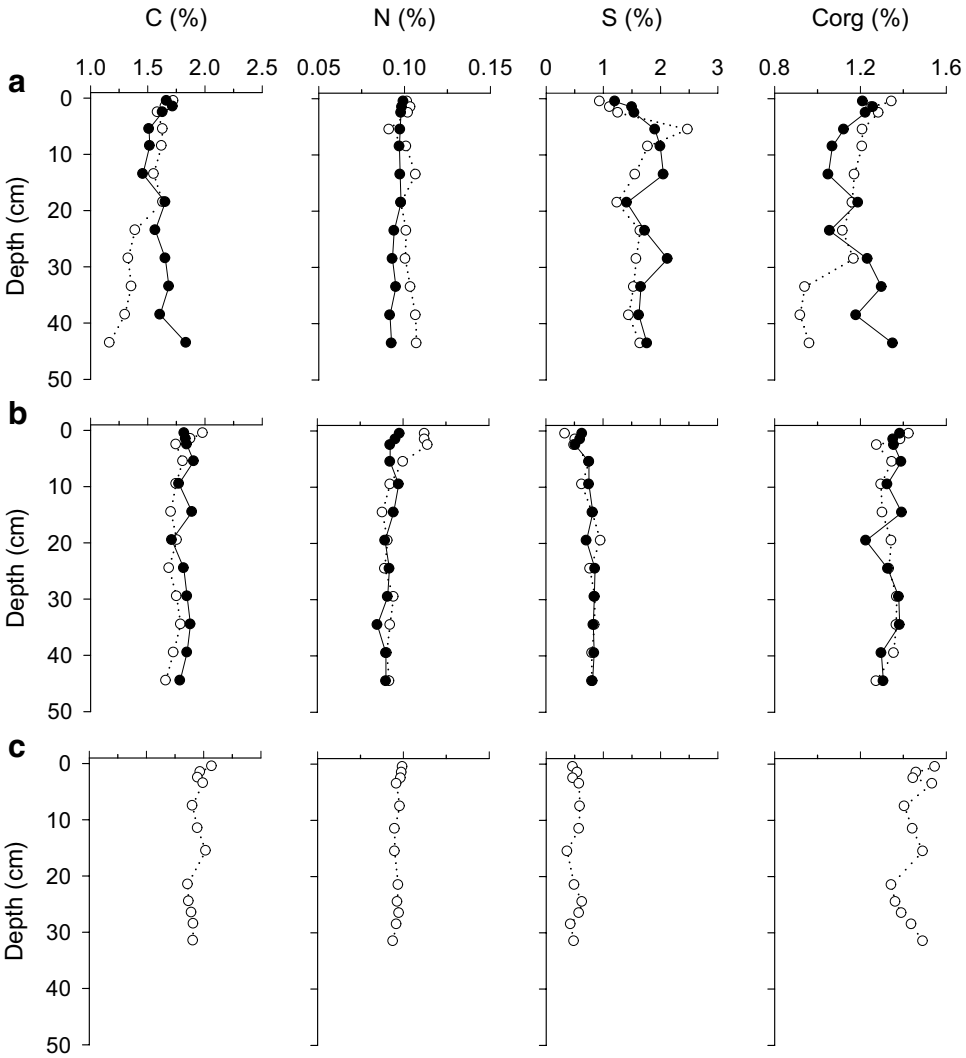

Fig. 5 Sediment profiles of carbon (C), nitrogen (N), sulphur (S) and organic carbon (C_{org}) measured in sediment samples of the cores retrieved in the cruises of June (white circles) and December (black circles) for the three MVs: Anastasya (**a**), Pipoca (**b**) and St. Petersburg (**c**)

Biogeochemical variables and diffusive fluxes

The vertical variation of TA and DIC (Fig. 7) in the sediment differed significantly between the three MVs. And the values in the pore water of the surface sediments resulted similar to those from bottom waters (with a mean difference of 11.4 ± 9.9% for TA and 11.3 ± 3.1% for DIC for all the MVs). Anastasya MV presented a considerable increase of these variables out of 13.5 cm, reaching maximum values of 7.8 mM for TA and 7.5 mM for DIC in June and 10.7 mM for TA and 10.6 mM for DIC in December. However, in the case of Pipoca MV, TA and DIC had a relatively constant behaviour with depth for both cruises (2.3 ± 0.2 mM and 2.1 ± 0.2 mM, respectively). St. Petersburg MV showed a sharp increase of TA and DIC in the bottom samples of the core, with values of 4.9 and 3.7 mM, respectively. pH at 20 ºC values showed significant differences among the MVs (Fig. 7), with slightly higher values in June than December for Anastasya and Pipoca MVs and maximum mean values (8.1 ± 0.2) for St. Petersburg MV. CH_4 concentrations were low and constant during June and December in Pipoca MV cores and in the upper sediments in Anastasya and St. Petersburg MVs (lower than 1.5 µM). The highest values in Anastasya MV were found in the middle zone of the core, with values of 19.3 µM (18.5 cm) in June and 44.2 µM (28.5 cm) in December. St. Petersburg MV presented the highest CH_4 concentration values, with values near to 80 µM at a depth of 40 cm approximately.

Nutrient concentrations in the first top centimetres of sediment were moderately enriched with respect to the bottom water, except for NO_3^- plus NO_2^- (Fig. 8). PO_4^{3-} presented significant differences between the MVs and also a distinct behaviour along the cores. Pipoca MV presented the greatest mean values in both cruises (5.5 ± 2.6 µM) and a gradual increase with depth. In Anastasya and St. Petersburg MVs, an increase of PO_4^{3-} was observed for the middle levels of the cores with a later decrease. NH_4^+ concentrations in pore water were significantly different among the MVs,

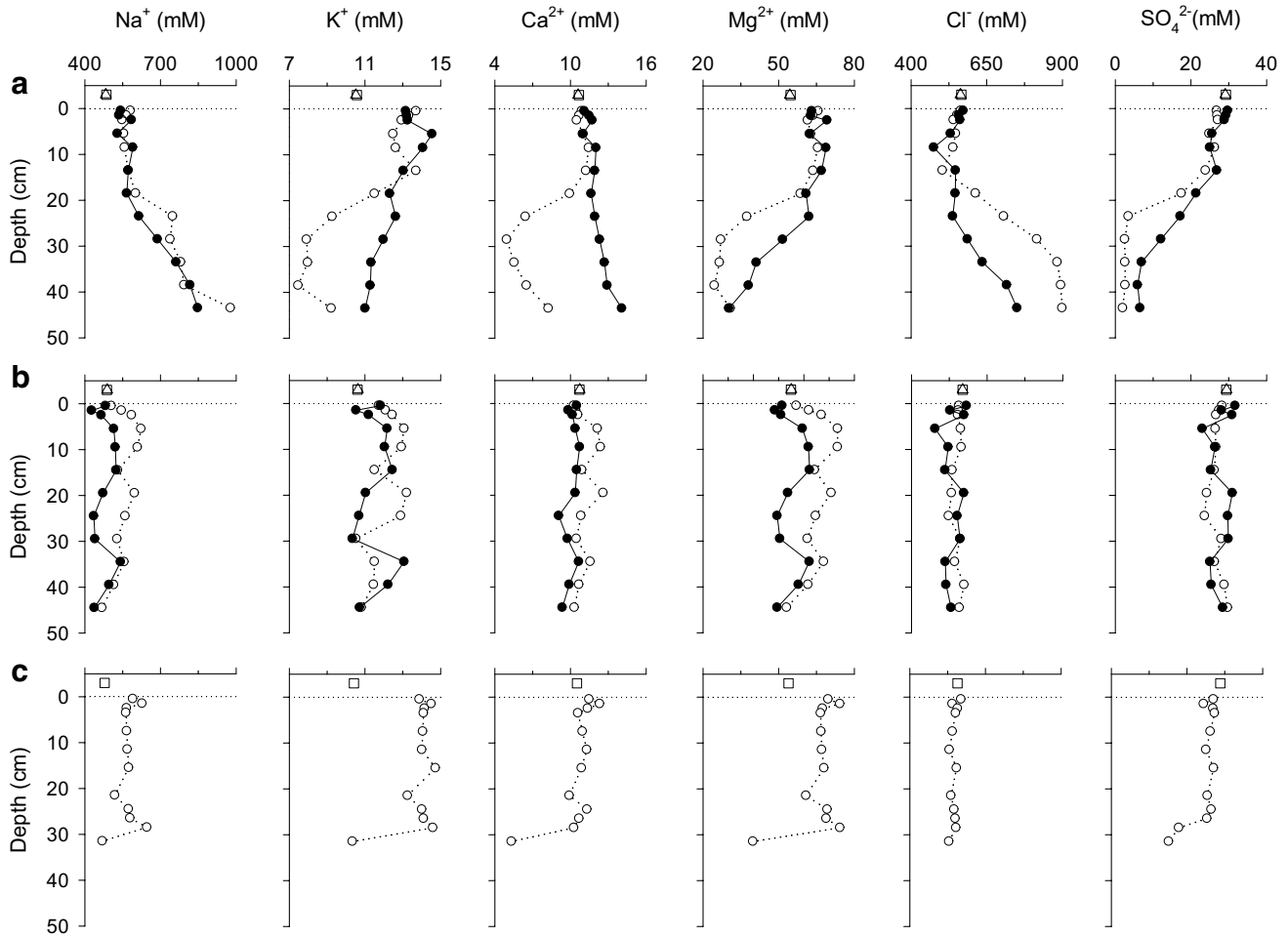

Fig. 6 Profiles of the concentration of Na^+, K^+, Ca^{2+}, Mg^{2+}, Cl^- and SO_4^{2-} measured in sediment samples of the cores retrieved in the cruises of June (white squares for bottom water and white circles for pore water) and December (white triangles for bottom water and black circles for pore water) for the three MVs: Anastasya (**a**), Pipoca (**b**) and St. Petersburg (**c**)

although they presented a similar behaviour along the cores in the case of Anastasya and St. Petersburg MVs. These MVs showed constant values of NH_4^+ in the top sediments, with mean values of 29.9 ± 5.1 and 22.6 ± 5.3 μM for both cruises, respectively. Towards the core bottom, these concentrations tended to increase up to 690.2 and 865.7 μM for Anastasya MV during June and December, respectively, and to 288.1 μM for St. Petersburg MV. However, Pipoca MV displayed constant concentrations of NH_4^+ along the cores in both cruises, with a mean value of 41.2 ± 7.1 μM. The concentration of NO_3^- plus NO_2^- showed significant differences for the three MVs, and it generally presented lower values in the first top centimetres of the sediment. The highest mean values were observed in St. Petersburg MV (7.4 ± 5.2 μM) and the lowest in Anastasya MV (4.1 ± 1.1 μM). Finally, N_2O concentrations (Fig. 8) also presented significant differences among the MVs, obtaining the greatest values of 0.90 ± 0.37 μM in the subsurface levels of the sediment (between core depths of 2 and 8 cm).

Table 3 shows the diffusive fluxes across the sediment–water interface estimated for PO_4^{3-},NH_4^+, NO_3^- plus NO_2^-, TA, DIC, CH_4 and N_2O (F PO_4^{3-}, F NH_4^+, F(NO_3^- +NO_2^-), FTA, FDIC, FCH_4 and FN_2O, respectively) for the three MVs. Positive fluxes indicate that the sediment acts as a source of the species to the water, whereas negative fluxes mean that the sediment acts as a sink. In general, there was no clear spatial or seasonal variation of the different diffusive fluxes in the MVs. The highest mean values of F PO_4^{3-} and FN_2O were obtained in Pipoca MV (0.42 ± 0.16 and 0.61 ± 0.17 μmol m^{-2} d^{-1}, respectively) and the lowest in Anastasya (0.19 ± 0.02 μmol m^{-2} d^{-1}) and St. Petersburg MVs (0.20 μmol m^{-2} d^{-1}), respectively. Moreover, Anastasya MV presented the greatest mean diffusive fluxes for NH_4^+, TA, DIC and CH_4, with values of 37.61 ± 6.03, 259.39 ± 30.90, 230.46 ± 82.82 and 0.42 ± 0.03 μmol m^{-2} d^{-1}, respectively, while the smallest values were determined for NH_4^+, TA and DIC in St. Petersburg MV (14.27, 57.80 and 25.69 μmol m^{-2} d^{-1}, respectively) and for CH_4 in

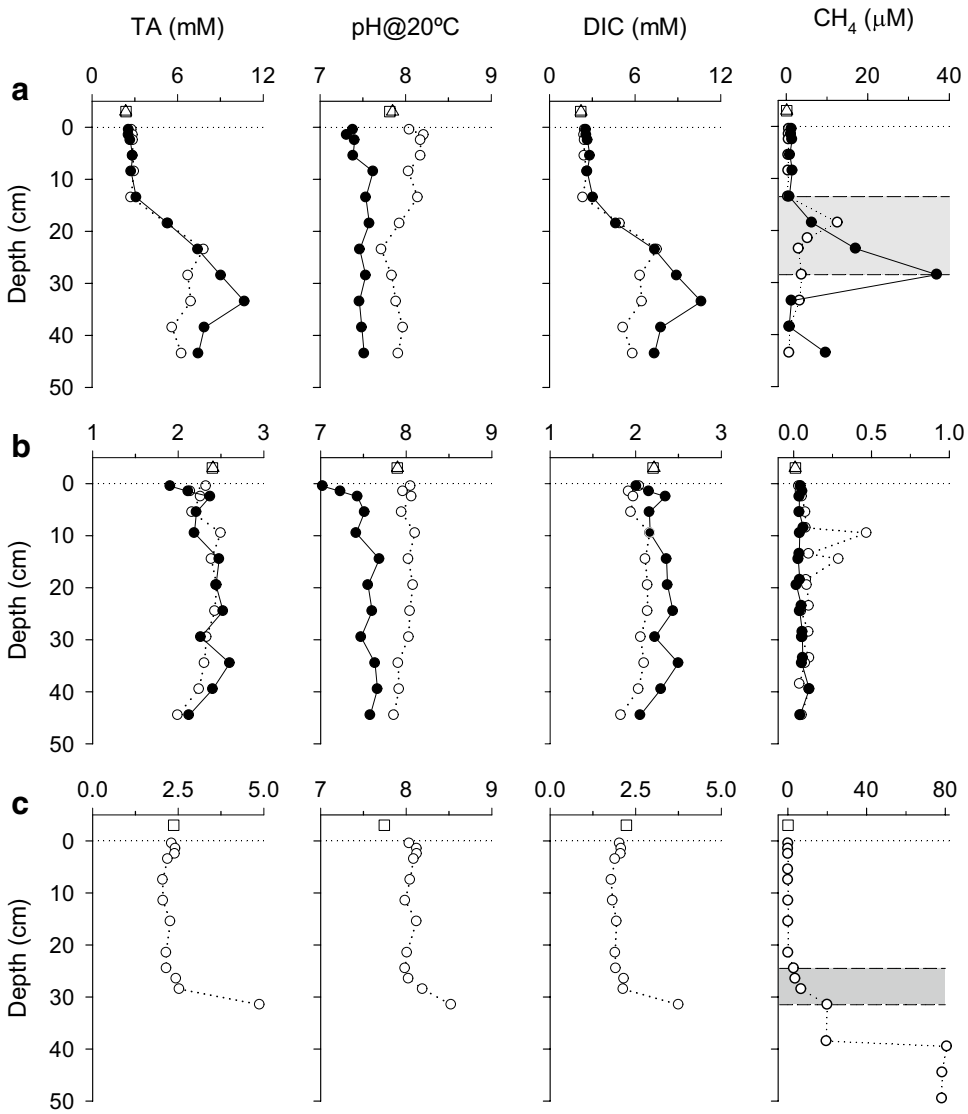

Fig. 7 Profiles of the concentration of total alkalinity (TA), normalized pH at 20 ºC (pH at 20 ºC), dissolved inorganic carbon (DIC) and methane (CH_4) measured in sediment samples of the cores retrieved in the cruises of June (white squares for bottom water and white circles for pore water) and December (white triangles for bottom water and black circles for pore water) for the three MVs: Anastasya (**a**), Pipoca (**b**) and St. Petersburg (**c**). Shaded zones in CH_4 profiles correspond to the sulphate–methane transition zone at the respective sites. Note the different scales used in some profiles

Pipoca MV (0.07 ± 0.04 µmol m^{-2} d^{-1}). $F(NO_3^-+NO_2^-)$ were similar in all the MVs, with resulting values between -5.55 and -6.95 µmol m^{-2} d^{-1}.

Discussion

Major elements

The behaviour of Na^+, K^+ and Cl^- concentrations in the pore water of Anastasya MV could be attributed to some of the mineral transformation reactions. The clay mineral dehydration, most likely by the conversion from smectite to illite, releases Na^+ from smectite interlayers and removes K^+, a required interlayer cation in illite (Fig. 6) (Perry and Hower, 1970; Hower et al., 1976; Martin et al., 1996; Hensen et al., 2007; Vanneste et al., 2011). Moreover, this process in turn can produce a reduction of Cl^- due to the freshwater contribution (Vanneste et al., 2011; Li et al., 2014). In our case, this effect was not observed (Fig. 6), as evidenced from the calculated values of salinization ratios (Fig. 9) that reflected an increase of salinity in the pore water of Anastasya MV from 13.5 to 23.5 cm core deep, approximately. The rises of Cl^- and Na^+ are also associated with the dissolution of halite (e.g. Kastner et al., 1990; Li et al., 2014), a process that normally overprints the signal of clay dehydration (Hensen et al., 2007). This would explain why the general behaviour caused by clay dehydration was not observed with clarity in the Anastasya MV profiles. The relative Na^+ and Cl^- enrichments could also be derived from the addition of NaCl (Bernasconi, 1999; Charlou et al., 2003; Reitz et al., 2007) and/or the interaction with evaporate deposits (brines) related to the diapiric structures associated to some MVs (Fernández-Puga et al., 2007; Huguen et al., 2009; Haffert et al., 2013; Dupré et al., 2014). The concentration distribution observed of Na^+, K^+ and Cl^- for Pipoca and St.

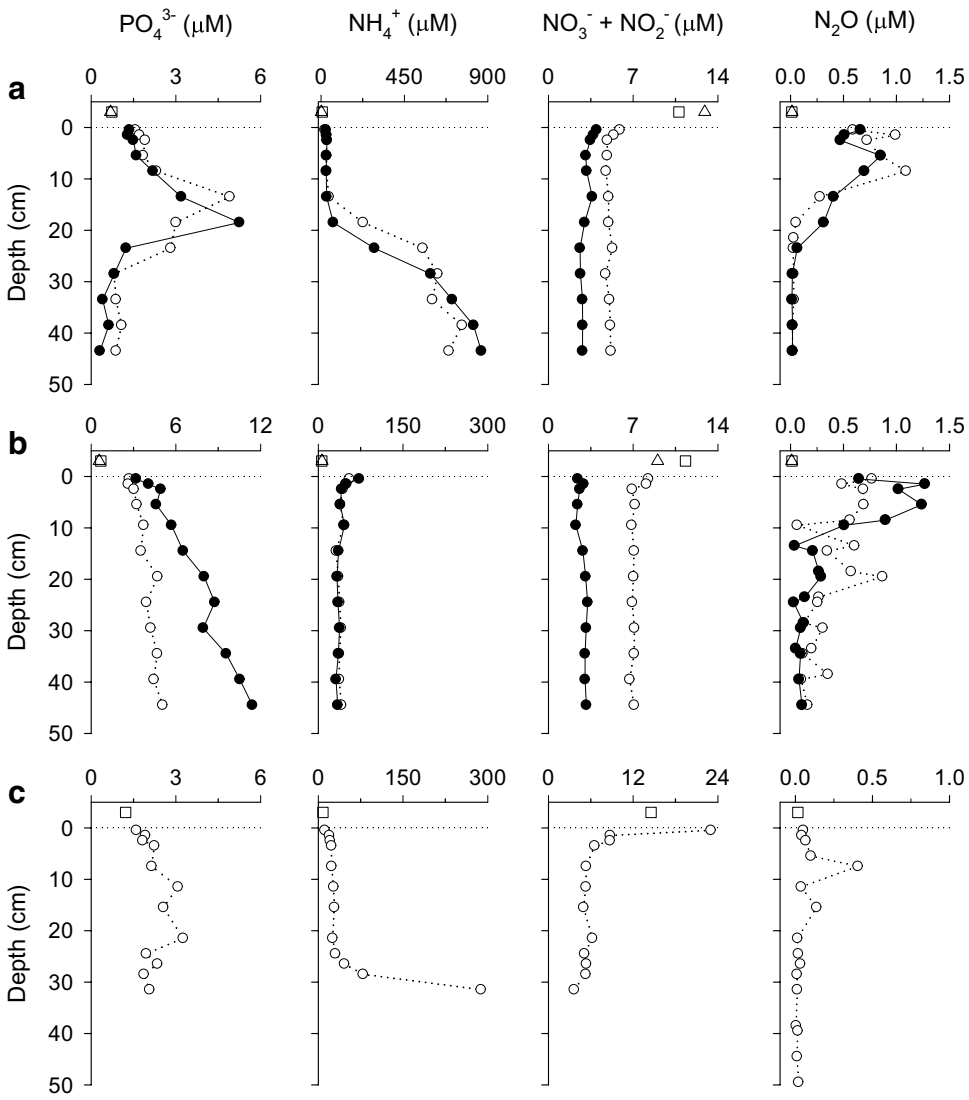

Fig. 8 Profiles of the concentration of PO_4^{3-}, NH_4^+, NO_3^- plus NO_2^- and nitrous oxide (N_2O) measured in sediment samples of the cores retrieved in the cruises of June (white squares for bottom water and white circles for pore water) and December (white triangles for bottom water and black circles for pore water) for the three MVs: Anastasya (**a**), Pipoca (**b**) and St. Petersburg (**c**). Note the different scales used in some profiles

Petersburg MVs (Fig. 6) did not show the presence of these mineral reactions in the sampled sediment.

However, the transformation from smectite to illite and the dissolution of halite are processes that usually take place in the deeper layers of the sedimentary column related to elevated temperatures (e.g. Martin et al., 1996; Vanneste et al., 2011). But the upward fluid movements produced by the escape pathway for overpressured material and fluids during periods of MV activity (Hensen et al., 2007; Medialdea et al., 2009; Palomino et al., 2016; Magalhaes et al.,

Table 3 Diffusive fluxes of PO_4^{3-}, NH_4^+, NO_3^- plus NO_2^-, total alkalinity (TA), dissolved inorganic carbon (DIC), methane (CH_4) and nitrous oxide (N_2O) across the sediment–water interface for the different MVs sampled (Anastasya, Pipoca and St. Petersburg) during the cruises of June and December

MV	Cruise	F PO_4^{3-}	F NH_4^+	F(NO_3^-+NO_2^-)	FTA	FDIC	FCH_4	FN_2O
Anastasya	June	0.17	33.3	−6.9	281	171	0.44	0.48
	December	0.20	41.9	−6.0	237	289	0.39	0.51
Pipoca	June	0.30	12.4	−5.6	60	54	0.04	0.49
	December	0.53	55.8	−6.9	440	372	0.10	0.73
St. Petersburg	June	0.32	14.3	−6.6	57	25	0.10	0.20

The fluxes are expressed in μmol m^{-2} d^{-1}

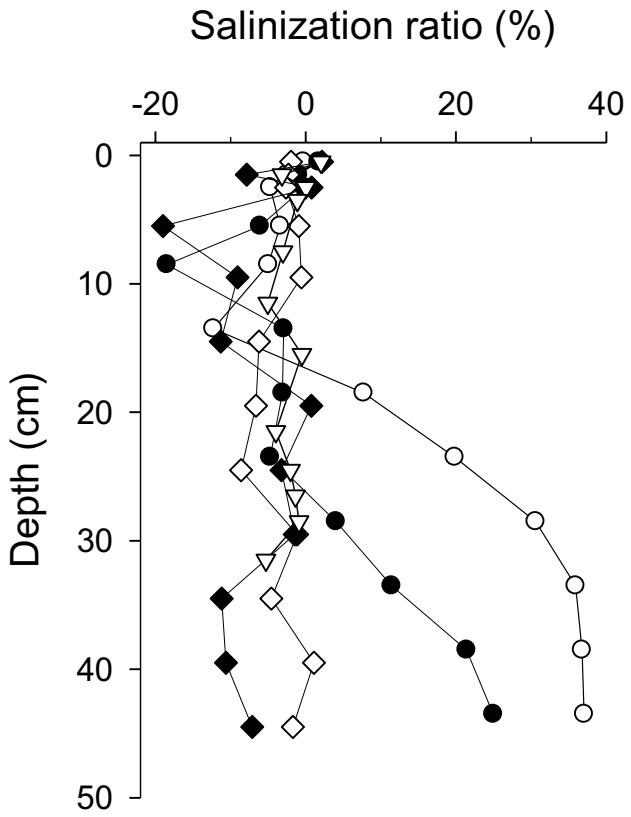

Fig. 9 Profiles of the salinization ratio of the three MVs sampled (Anastasya (circles), Pipoca (diamonds) and St. Petersburg (triangles)) during June (white fill) and December (black fill)

2019) may relocate these changes in shallower layers of the sediment. In this respect, a preliminary approximated range value of upward fluid flow has been estimated through the relative conservative behaviour found between Na^+ and Cl^- in Anastasya MV ($r^2 = 0.82 \pm 0.05$) for the depths at which the vertical variations of Na^+ and Cl^- were observed (below 13.5 in June and 18.5 cm in December) (Fig. 10). The flow velocities calculated resulted between 2 and 5 cm $year^{-1}$, being within the interval considered as moderate activity of the MV systems in the GoC (Hensen et al., 2007) and in the eastern Mediterranean (Haese et al., 2003, 2006). Pipoca MV did not show experimental evidence of cold seep transport, and the vertical variations of Na^+ and Cl^- in St. Petersburg MV only showed changes at the bottom level of the core, which may be also reflecting the existence of inactivity periods in these two MVs.

The decrease in Ca^{2+} and Mg^{2+} concentrations in the pore water (Fig. 6) is usually produced by the authigenic carbonate mineral precipitation reactions (Kastner et al., 1990; Martin et al., 1996; Loyd and Berelson, 2016), such as the direct crystallization of calcite and dolomite, the recrystallization of calcite to dolomite and the addition of Mg^{2+} to dolomite (Baker and Burns, 1985). In this work, pore water profiles show a more evident decrease in Mg^{2+} than Ca^{2+} concentrations in Anastasya and St. Petersburg MVs, even with a slight increase of Ca^{2+} in December for Anastasya MV. The coupled decreases of Ca^{2+} and Mg^{2+} in the profiles may point out the direct precipitation of calcite and dolomite, and the progressive decreases in Mg^{2+} content at deeper sediment levels are indicative of dolomite replacement reactions or the addition of Mg^{2+} to dolomite. A similar distribution in sediments along the western continental margins around the world (Cascadia, Peru and southern Africa) was observed by Loyd and Berelson (2016). Moreover, the authigenic carbonate precipitation can be displayed with the behaviour of the ion activity product (IAP) of calcite and dolomite at different sediment depths (Moore et al., 2004; Wehrmann et al., 2011). If IAP is higher than K_{sp} (solubility product constant), the solution is oversaturated, and the mineral begins to precipitate. In order to calculate the IAP of these minerals, it is necessary to have the concentrations and activity coefficients of Ca^{2+}, Mg^{2+} and DIC according to Hu et al. (2017) and the references included therein. In Anastasya and St. Petersburg MVs, log IAP values of calcite and dolomite calculated along all the cores were of ~ − 6.77 to − 6.60 and ~ − 12.87 to − 12.27, respectively. These values resulted higher than log $K_{sp\text{-}Calcite}$, − 8.48 (Schulz, 2006), and log $K_{sp\text{-}Dolomite}$, − 16.52 (Moore et al., 2004), at 25 °C and standard atmospheric pressure. This demonstrates the possibility of calcite and dolomite precipitations coupled to Ca^{2+} and Mg^{2+} depletions. Log IAP values also presented a general increase with core depth except for Anastasya MV in the deeper levels of the sediment during December, being related to the increase of Ca^{2+} concentrations observed. Hu et al. (2017) also found in the offshore sediments in southwestern Taiwan the possibility of dolomite precipitation coupled to Ca^{2+} and Mg^{2+} decreases in pore water, and they believed that this could be correlated to microbially mediated dolomite formation by sulphate-reducing bacteria (Vasconcelos et al., 1995; Warthmann et al., 2000).

Diagenetic processes

The diagenetic processes in sediment proceed via a vertical zonation based on the sequential utilization of terminal electron acceptors available for organic matter oxidation (e.g. Emerson et al., 1980; Arndt et al., 2013). The aerobic oxidation of the organic matter confined to the oxic zone takes place in the sediment surface and produces a decrease in C_{org} (Jørgensen and Revsbech, 1989; Rabouille and Gaillard, 1991), as observed in the three MVs studied (Fig. 5). Oxygen is also consumed in this zone through the oxidation of reduced compounds as the NH_4^+ in the process of nitrification (Soetaert et al., 1996; Sarmiento and Gruber, 2004), which is associated with both the highest surface concentrations of NO_3^- and the lowest content of NH_4^+ in Anastasya

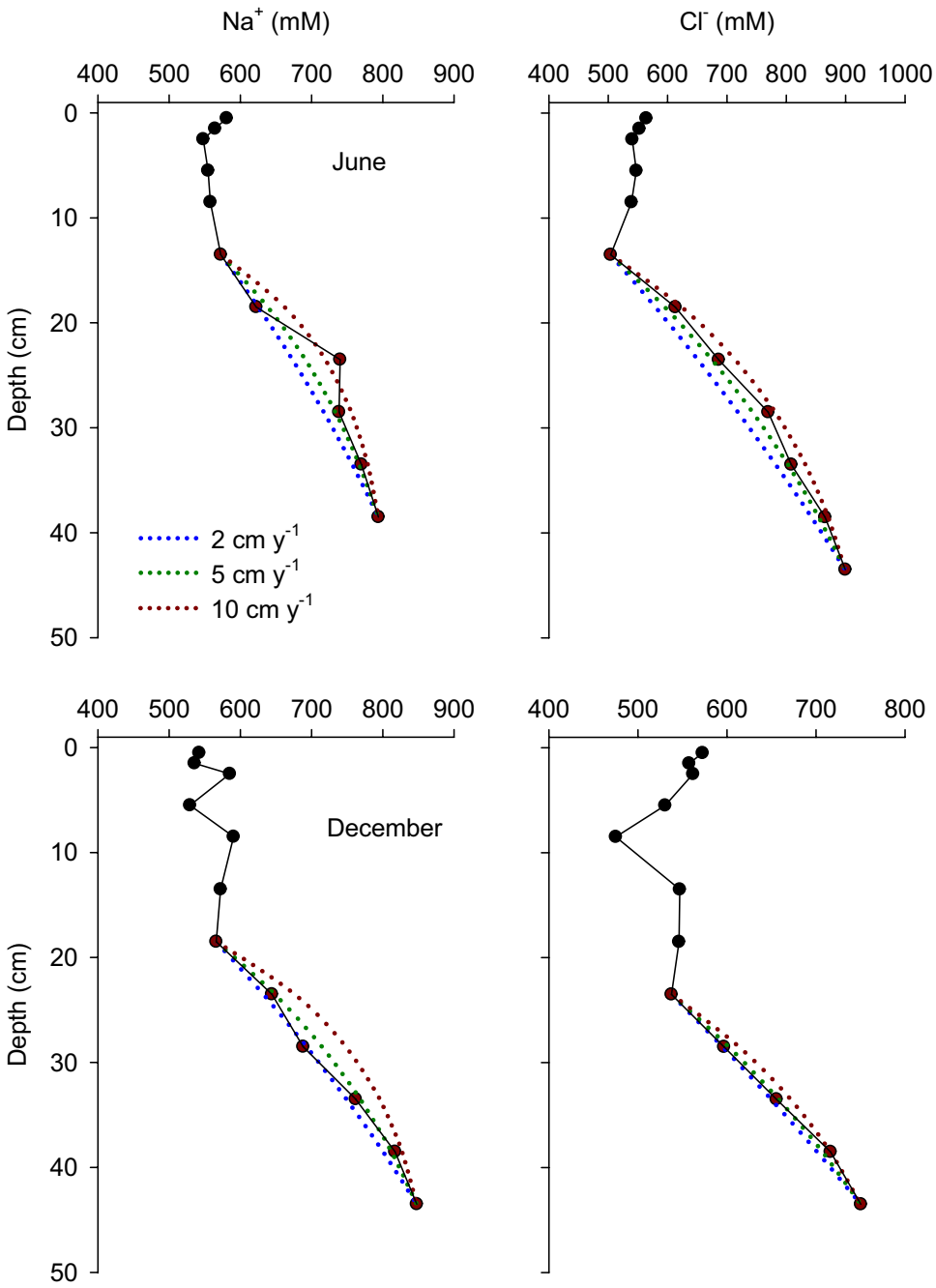

Fig. 10 Simulations of the vertical profiles of conservative solutes (Na^+ and Cl^-) accounting for variable advective flow velocities (2, 5 and 10 cm $year^{-1}$) for Anastasya MV cores in June and December cruises

and St. Petersburg MVs. However, Pipoca MV presented the highest concentrations of NH_4^+ in the surface sediments, suggesting that there is a coupling between nitrification and another process generated when the oxygen is consumed, such as nitrate reduction or denitrification (Froelich et al., 1979; Krumins et al., 2013). Both processes generate N_2O as a by-product that would explain the N_2O concentration peaks observed in the first top centimetres of all the MVs studied (Fig. 8).

Below the oxic zone, the sulphate reduction becomes an important diagenetic process in the sediment, since the dissolved sulphate is one of the main electron acceptors available for the oxidation of organic matter in marine sediments (Borowski et al., 1999; Kastner et al., 2008; Luo et al., 2013). The result is a decrease of SO_4^{2-} (Fig. 6) and an increase of TA and DIC (Fig. 7) that can be observed in Anastasya and St. Petersburg MVs, while in Pipoca MV, the profiles stayed practically constant. This is also corroborated by the negative linear correlations observed between the variations of DIC and SO_4^{2-} concentrations, very similar in both Anastasya ($r^2 = 0.67$) and St. Petersburg MVs ($r^2 = 0.65$) but negligible in the case of Pipoca

MV. In addition, the relationship between the consumption of sulphate (ΔSO_4^{2-}) and the production of DIC (ΔDIC) may indicate the nature of the oxidation process that fuels sulphate reduction (Haese et al., 2003; Coffin et al., 2008; Kastner et al., 2008; Luo et al., 2013). The dissolved sulphate in pore water participates in two main processes serving as the major electron acceptor for organic matter remineralization in the sediment. First of all, the organoclastic sulphate reduction (OSR) that plays a critical role in the early diagenesis of marine sediments and produces 2 mol of bicarbonate per mole of sulphate reduced $2CH_2O + SO_4^{2-} \rightarrow 2\,HCO_3^- + H_2S$ (Brener 1980), and secondly, the AOM coupled sulphate reduction that produces 1 mol of bicarbonate per mole of sulphate reduced $CH_4 + SO_4^{2-} \rightarrow HCO_3^- + HS^- + H_2O$ and is mediated by methanotrophic archaea and sulphate-bearing sediments (Boetius et al., 2000; Orphan et al., 2001). When these processes take place, the concentration of DIC in the pore water increases and therefore also does TA, which facilitates the precipitation of authigenic carbonate minerals (Peckmann et al., 2001). This precipitation tends to be accompanied with a decrease in Ca^{2+} and Mg^{2+} concentrations, as described in the previous section, and the total DIC produced by sulphate reduction must be corrected for Ca^{2+} and Mg^{2+} incorporation into authigenic carbonates ($\Delta DIC + \Delta(Ca^{2+} + Mg^{2+})$) (Luo et al., 2013; Hu et al., 2015). Figure 11 shows adjusted DIC with the Ca^{2+} and Mg^{2+} concentrations added versus sulphate removed (all data are result of the differences between the bottom water and the measured pore water concentrations) by the different sediment facies observed (hemipelagic and mud breccia) and the mousse-like texture in Anastasya and St. Petersburg MVs. In this study, Pipoca MV was not represented because the relationship between DIC and SO_4^{2-} was negligible. Diagonal solid and dotted lines in Fig. 11 indicate the established ratios of $\Delta DIC + \Delta(Ca^{2+} + Mg^{2+})$: ΔSO_4^{2-}. The data were not clearly distributed along these lines for both MVs, although certain relation appeared evident in the case of Anastasya MV. Thus, in the plot of Anastasya MV (Fig. 11a), four slopes were displayed, 0.4:1, 1:1 (AOM), 2:1 (OSR) and 5:1, in addition to the two main sediment facies as well as the mousse-like texture placed in each slope. Hemipelagic sediment data was plotted near the 5:1 slope, indicating that sulphate reduction was caused by OSR, the mud breccia was clustered among the 1:1 and 2:1 slopes and close to 5:1 suggesting that the decreased sulphate concentration was produced by both OSR and AOM, and finally, the mousse-like texture was plotted near the 0.4:1 and 1:1 slopes, which was related to AOM process. The data for St. Petersburg MV are shown in Fig. 11b, where three slopes were indicated, 5:1, 2:1 and 1:1. The facies of hemipelagic sediment and mud breccia are near to the 5:1 slope, showing a greater influence of OSR in the sulphate reduction, and the mousse-like texture is distributed between the 1:1 and 2:1 slopes, reflecting the presence of AOM and OSR processes.

In anoxic sediments when other electron acceptors like NO_3^- or SO_4^{2-} ions are depleted, methanogenesis takes place. In this process, CH_4 is produced by anaerobic methanogenic archaea as the end product of the degradation of organic matter (Martens and Berner, 1974; Canfield et al., 2005). In Anastasya and St. Petersburg MVs, an increase of CH_4 coupled with a decrease of SO_4^{2-} (Figs. 6 and 7) was detected in an area inside the sediments that is known as the

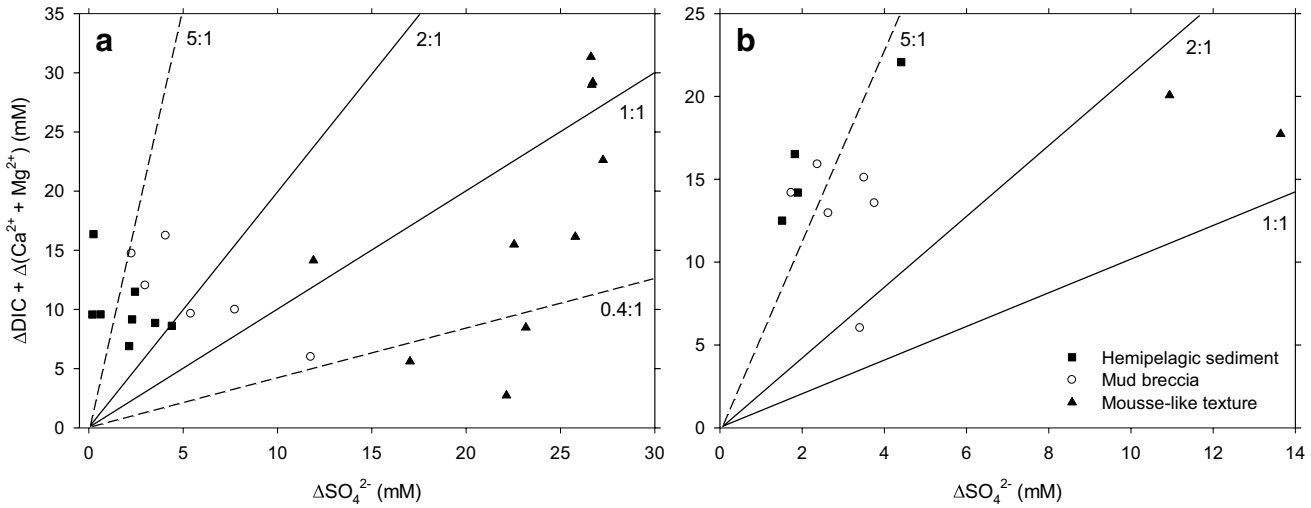

Fig. 11 Plots of consumed sulphate ($\Delta\ SO_4^{2-}$) versus DIC produced, corrected for Ca^{2+} and Mg^{2+} to account for the precipitation of authigenic carbonate minerals ($\Delta DIC + \Delta(Ca^{2+} + Mg^{2+})$) for the different sediment facies observed (hemipelagic and mud breccia) and the mousse-like texture in the MVs of Anastasya (**a**) and St. Petersburg (**b**). Diagonal lines represent the 5:1, 2:1, 1:1 and 0.4:1 ratios of $\Delta DIC + \Delta(Ca^{2+} + Mg^{2+})$, where 1:1 reflects sulphate reduction related to the process of anaerobic oxidation of methane (AOM), whereas a ratio of 2:1 reflects sulphate reduction related to organoclastic sulphate reduction (OSR)

sulphate–methane transition zone (SMTZ) (e.g. Lee et al., 2018; Akam et al., 2020). Feng et al. (2018) observed in the Beikang Basin of the southern South China Sea that the dissolved SO_4^{2-} was predominantly consumed by the AOM and consequently almost all the CH_4 sourced from subsurface sediments was depleted within the SMTZ, resulting in low CH_4 diffusive fluxes (0.16–0.41 nmol m^{-2} d^{-1}). Egger et al. (2018) analysed the depth of this SMTZ in different marine sediments, and they determined that for slope areas, it was deeper (1280 ± 1210 cm sediment depth). The SMTZ in our study resulted shallower (13.5 cm in Anastasya MV and 24.5 cm in St. Petersburg MV), which can also reveal the importance of the fluid migration in this systems.

Moreover, NH_4^+ concentrations showed an increase with depth in Anastasya and St. Petersburg MVs (Fig. 8), probably due to the release of nitrogen from the organic matter of its own bacterial action in reduced conditions (Berg et al., 1998), in addition to other processes such as sulphate reduction and methanogenesis. The profiles also presented a general increase of PO_4^{3-}, although these concentrations were generally low in the three MVs due to its own adsorption processes that happen in the sediment (Krom and Berner, 1980). Anastasya and St. Petersburg MVs showed a progressive rise derived from the degradation of organic matter (e.g. Jensen et al. 1995; Canfield et al., 2005) up to the depth at which the mousse-like texture is located with a subsequent decrease. This last behaviour reflects a removal of PO_4^{3-} of the pore water by different processes, such as the adsorption on the sediment and the in situ transformation into a mineralized form, as the fluorapatite, a process generated at a certain depth inside the sediment (Schuffert et al., 1998; Sasaki et al., 2001). However, a mousse-like texture was not identified in the case of Pipoca MV, and the PO_4^{3-} concentrations increased gradually with depth by this degradation of the organic matter.

Diffusive fluxes of phosphorus, nitrogen and inorganic carbon

There is little information available about diffusive fluxes in the sediment of marine systems at depths greater than 100 m of the water column (Boynton et al., 2017); most of the databases found are referred to shallow areas (e.g. Boynton and Ceballos, 2017). However, previous studies have described the existence of a general decrease of the diffusive fluxes with the increase of the depth of the water column (Boynton et al., 2017) together with the decrease of the amount of organic matter in the sediments of continental shelves (Berelson et al., 2003). Moreover, these benthic diffusive fluxes are usually lower than those obtained with other measurement techniques, such as benthic chambers and/or core incubations in the laboratory (Cermelj et al., 1997; Berelson et al., 2003). The differences have been related in many studies with the important role of the irrigation produced by the benthic macrofauna about the exchange of compounds between the sediment and water column (Cermelj et al., 1997).

The light concentration variation observed in the vertical profiles of inorganic carbon and nutrients in the surface hemipelagic sediments (Figs. 7 and 8) produce a low exchange of these species between sediment and bottom water in the three MVs. In general, the estimation values of these diffusive fluxes could be considered relatively low (Table 3) compared to those described for sediments of continental slopes around the world. PO_4^{3-} fluxes are low (0.17–0.53 µmol m^{-2} d^{-1}), but they are within the range of variation calculated by Hensen et al. (2000) in deep sediments of the northern Cape basin in South Africa. On the other hand, the NH_4^+ fluxes values ranged between 12.4 and 55.8 µmol m^{-2} d^{-1} and resulted similar to those found by Denis et al. (2001) in the NW Mediterranean. The sediments act as a sink for NO_3^- plus NO_2^- in the three MVs, with relatively constant fluxes between − 5.6 and − 7.0 µmol m^{-2} d^{-1}. The magnitude produced from this NO_3^- exchange with the marine sediments is associated with the intensity of the denitrification processes (e.g. Christensen et al., 1987), and these diffusive fluxes have been described within a wide range of variation in different marine areas (500–4800 m), with both negative and positive values (Brunnegard et al., 2004; Trimmer and Nicholls, 2009). DIC diffusive fluxes ranged between 172–289, 54–373 and 26 µmol m^{-2} d^{-1} in Anastasya, Pipoca and St. Petersburg MVs, respectively. These values are similar to those found by Xu et al. (2018) in stations close to MVs in the western slope of the Mid-Okinawa Trough as well as by Hu et al. (2017) in several geological regions offshore southwestern Taiwan.

The measured diffusive fluxes of the greenhouse gases in the three MVs of this study are positive and indicate that the sediments act as a source of CH_4 and N_2O to the bottom waters of the GoC (Table 3). CH_4 fluxes varied between 0.04 and 0.44 µmol m^{-2} d^{-1}, and they are within the range of variation of the diffusive fluxes determined by Lin et al. (2006) and Xu et al. (2018) in Good Weather Ridge (Southwestern Taiwan) and in the western slope of the Mid-Okinawa Trough, respectively. N_2O fluxes presented values ranging between 0.20 and 0.73 µmol m^{-2} d^{-1} and result similar to those described by Usui et al. (1998) in different marine systems (continental shelf of the East China Sea, Koaziro Bay, Equatorial Pacific and Subtropical North Pacific).

In addition, the weak variation observed in the concentration of the chemical species in the surface sediments suggests the existence of another transport mechanism in the pore water, apart from its own biogeochemical processes, such as the presence of irrigation produced by the benthic macrofauna, the mixing effect by the action of bottom

currents and/or the upward fluid movements. The benthic macrofauna tends to homogenize the surface sediment layer by means of an intensification of the transport processes through the burrows (e.g. Aller, 1980). Thus, the cold seeps favour environments in which a large benthic macrofauna is developed and is also associated with chemosynthetic bacteria (Sibuet and Olu, 1998). Rueda et al. (2016) found in the three MVs studied in this work chemosynthesis-based communities associated with the anoxic mud breccia and the presence of bacterial mats along with the abundance of *Siboglinum* sp., *Lucinoma asapheus*, *Acharax gadirae*, *Solemya elarraichensis* and *Calliax* sp. Similarly, Palomino et al. (2016) also identified that these chemosynthesis-based communities are closely related to fluid seepage in MVs of the GoC, obtaining in Anastasya MV greater densities of macrofauna than in Pipoca MV.

The mixing of the surface sediments including the pore water can also be influenced by the bottom currents (Hensen et al., 2003). Pipoca MV is located in the proximity of the contourite channel where the Mediterranean Outflow Water (MOW) reaches a maximum speed of 0.3–0.5 m s^{-1}, while Anastasya MV is placed in a more protected area of this bottom current, with a maximum speed of 0.2 m s^{-1} (Fernández-Salas et al., 2012; Díaz-del-Río et al., 2014; Lozano et al., 2020). In this way, the thickness of the hemipelagic sediments over the mud breccia seems to have some relation with the bottom current intensities in Pipoca and Anastasya MVs.

Haese et al. (2006) also determined that the vertical gradients of solutes in the pore water of surface sediments can also be affected by gas bubbling or fluid convection. In the GoC, Sierra et al. (2020) analysed the vertical profiles of CH_4 concentration in the water column above the three MVs studied in this work and found a general increase towards deeper waters of the water column with values of 10–15 nmol L^{-1} in St. Petersburg MV and 100–125 nmol L^{-1} in Anastasya MV, whereas in Pipoca MV, this behaviour near to the bottom water was not observed. Additionally, Sierra et al. (2020) also studied the stable carbon isotope composition ($\delta^{13}C$) of dissolved CH_4 and pointed out less negative values in Anastasya and St. Petersburg MVs (−36.8 and −35.0‰, respectively), which can suggest that the emissions from cold seeps are more important than in the case of Pipoca MV (−42.5‰), where CH_4 seemed to have a biogeochemical origin. The effect of the MVs emissions over the concentration and isotope composition of CH_4 in deep waters is coherent with the changes of composition observed in the pore water of the sediment in the study area.

In the GoC, high CH_4 fluxes have also been described from deeper and relatively active MVs. For example, Vanneste et al. (2011) estimated maximum values of 2200 µmol m^{-2} d^{-1} in the Carlos Ribeiro MV (2170–2340 m water depth) using pore-fluid modelling. Sommer et al. (2008, 2009) measured in situ CH_4 fluxes with a benthic chamber under constant oxygen conditions with values between 0 and 600 µmol m^{-2} d^{-1} in the Captain Arutyunov MV (1321 m water depth). These fluxes reflect that zones with MVs can be considered as hotspots of CH_4 emissions to the oceans. This has already been pointed out by several works about submarine volcanism sites, such as the Arabian Sea (Jayakumar et al., 2001), the northwestern Black Sea (Amouroux et al., 2002) and the GoC (Sierra et al., 2020). Therefore, MVs should also be considered as a source of CH_4 to the atmosphere (Wallmann et al., 2006), with an estimated flux range between 13.3 and 26.7% with respect to the total oceanic CH_4 emissions (Weber et al., 2019).

Finally, the upward fluid movement observed in these structures could improve the transfer through the sediment. An estimation of this effect can be leaded by considering the advective fluxes calculated in Anastasya MV for the different species in the surface layer. Thus, it has been calculated, as these fluxes are usually lower than diffusive fluxes and they represent around 42.9 ± 5.1, 5.6 ± 0.1, 7.9 ± 1.6, 47.7 ± 4.9, 18.1 ± 8.0 and 10.7 ± 0.3% of the total fluxes estimated in this work across the sediment–water interface for PO_4^{3-}, NH_4^+, NO_3^- plus NO_2^-, inorganic carbon, CH_4 and N_2O, respectively.

Conclusions

The surficial sedimentary column in Anastasya, Pipoca and St. Petersburg MVs is characterized by a top hemipelagic layer overlaying mud breccia deposits. Moreover, a mousse-like texture was identified at the deepest level of the core record in Anastasya and St. Petersburg MV mud breccia sediments. The presence of this texture seems to control the distribution of some species studied (major elements, inorganic carbon and nutrients), since the vertical gradients begin to intensify from this depth in Anastasya and St. Petersburg MVs. This behaviour could be also attributed to the trend of the fluid leaking activity, i.e. Anastasya MV > St. Petersburg MV > Pipoca MV, which has been identified by means of different variables, such as the advection speed of the fluid in the sediment, the intensity of the CH_4 fluxes across the sediment and the CH_4 concentrations in the bottom water. The emplacement of certain species has allowed to distinguish several important processes, as the mineral transformation reactions in Anastasya MV and the sulphate reduction associated to the organic matter oxidation in Anastasya and St. Petersburg MVs. Conversely, the surficial sediment recovered in Pipoca MV has shown almost constant values with depth, which makes it difficult to identify any of these processes.

In general, most of the profiles in the three MVs were relatively constant in the shallow layers of the sediment,

derived mainly from the irrigation produced by the high benthic macrofauna present in these structures. This produces similar diffusive fluxes of phosphorus, nitrogen and inorganic carbon in our study area, with values near to other deep areas around the world. Furthermore, the sampled MVs can be considered as a source of CH_4 to the water column, with the greatest emission values in Anastasya MV (0.51 ± 0.01 µmol m^{-2} d^{-1}), followed by St. Petersburg MV (0.10 µmol m^{-2} d^{-1}) and Pipoca MV (0.07 ± 0.04 µmol m^{-2} d^{-1}).

Acknowledgements The authors would like to thank the crews of the R/V's Angeles Alvariño and Ramón Margalef for their assistance during fieldwork. We also thank the two anonymous reviewers and to the editor for the comments they provided, which helped substantially improve this article.

Funding This work was funded by the Spanish CICYT (Spanish Program for Science and Technology) under the contract RTI2018-100865-B-C21. Dolores Jiménez-López was financed by the University of Cádiz with a FPI fellowship (FPI-UCA), and Ana Sierra was financed by the Spanish Ministry of Education with a FPU fellowship (FPU2014-04048).

Data availability The datasets generated during and/or analysed during the current study are not publicly available but are available from the corresponding author on reasonable request.

Declarations

Competing interests The authors declare no competing interests.

References

Akam SA, Coffin RB, Abdulla HAN, Lyons TW (2020) Dissolved inorganic carbon pump in methane-charged shallow marine sediments: state of the art and new model perspectives. Front Mar Sci 7:1–13. https://doi.org/10.3389/fmars.2020.00206

Aller RC (1980) Quantifying solute distributions in the bioturbated zone of marine sediments by defining an average microenvironment. Geochim Cosmochim Acta 44:1955–1965. https://doi.org/10.1016/0016-7037(80)90195-7

Aloisi G, Bouloubassi I, Heijs SK, Pancost RD, Pierre C, Damsté JSS, Gottschal JC, Forney LJ, Rouchy J-M (2002) CH_4 consuming microorganisms and the formation of carbonate crusts at cold seeps. Earth Planet Sci Lett 203:195–203. https://doi.org/10.1016/S0012-821X(02)00878-6

Aloisi G, Drews M, Wallmann K, Bohrmann G (2004) Fluid expulsion from the Dvurechensky mud volcano (Black Sea). Part I. Fluid sources and relevance to Li, B, Sr, I and dissolved inorganic nitrogen cycles. Earth Planet Sci Lett 225:347–363. https://doi.org/10.1016/j.epsl.2004.07.006

Amouroux D, Roberts G, Rapsomanikis S, Andreae MO (2002) Biogenic gas (CH_4, N_2O, DMS) emission to the atmosphere from near-shore and shelf waters of the north-western Black Sea. Estuar Coast Shelf Sci 54:575–587. https://doi.org/10.1006/ecss.2000.0666

Arndt S, Jørgensen BB, LaRowe DE, Middelburg JJ, Pancost RD, Regnier P (2013) Quantifying the degradation of organic matter in marine sediments: a review and synthesis. Earth-Sci Rev 123:53–86. https://doi.org/10.1016/j.earscirev.2013.02.008

Baker PA, Burns SJ (1985) Occurrence and formation of dolomite in organic-rich continental margin sediments. Am Assoc Petrol Geol Bull 69:1917–1930

Bakker DCE, Bange H, Gruber G, Johannessen T, Upstill-Goddard RC, Borges AV, Delille B, Loscher CR, Naqvi SWA, Omar AMS, Santana-Casiano JM (2014) Air-sea interactions of natural long-lived greenhouse gases (CO_2, N_2O, CH_4) in a changing climate. In: Liss, P.S. and Johnson, M. T. (eds) Ocean-atmosphere interactions of gases and particles. Springer Verlag, pp. 113–169. https://doi.org/10.1007/978-3-642-25643-1

Berelson WM, McManus J, Coale KH, Johnson KS, Burdige DJ, Kilgore T, Colodner D, Chavez FP, Kudela R, Boucher J (2003) A time series of benthic flux measurements from Monterey Bay, CA. Cont Shelf Res 23:457–481. https://doi.org/10.1016/S0278-4343(03)00009-8

Berg P, Risgaard-Petersen N, Rysgaard S (1998) Interpretation of measured concentration profiles in sediment pore water. Limnol Oceanogr 43:1500–1510. https://doi.org/10.4319/lo.1998.43.7.1500

Bernasconi SM (1999) Interstitial water chemistry in the Western Mediterranean: results from Leg 161. Proc Ocean Drill Progr Sci Results 161:423–432. https://doi.org/10.2973/odp.proc.sr.161.228.1999

Berner RA (1980) Early diagenesis: a theoretical approach. Princeton University Press, Princeton, pp. 241. https://doi.org/10.1017/S0016756800035962

Boetius A, Ferdelmann T, Lochte K (2000) Bacterial activity in sediments of the deep Arabian Sea in relation to vertical flux. Deep Sea Res Part II: Top Stud Oceanogr 47:2835–2875. https://doi.org/10.1016/S0967-0645(00)00051-5

Borowski WS, Paull CK, Ussler W (1996) Marine pore-water sulfate profiles indicate in situ methane flux from underlying gas hydrate. Geology 24:655–658. https://doi.org/10.1130/0091-7613(1996)024%3c0655:MPWSPI%3e2.3.CO;2

Borowski WS, Paull CK, Ussler W (1999) Global and local variations of interstitial sulfate gradients in deep-water, continental margin sediments: sensitivity to underlying methane and gas hydrates. Mar Geol 159:131–154. https://doi.org/10.1016/S0025-3227(99)00004-3

Boudreau BP (1997) Diagenetic models and their implementation: modelling transport and reactions in aquatic sediments. Springer-Verlag, Berlin, pp. 414. https://doi.org/10.1017/S0016756897217656

Boynton WR, Ceballos MA (2017) World Flux Data Set 2016. Mendeley Data, v3. https://doi.org/10.17632/8gc3ys3jx6.3

Boynton WR, Ceballos MAC, Bailey EM, Hodgkins CLS, Humphrey JL, Testa JM (2017) Oxygen and nutrient exchanges at the sediment-water interface: a global synthesis and critique of estuarine and coastal data. Estuar Coast 41:301–333. https://doi.org/10.1007/s12237-017-0275-5

Brener RA (1980) Early diagenesis: a theoretical approach. Princeton University Press, pp. 256

Broecker WS, Peng TH (1974) Gas exchange rates between air and sea. Tellus 26:21–35. https://doi.org/10.3402/tellusa.v26i1-2.9733

Brown KM (1990) The nature and hydrogeologic significance of mud diapirs and diatremes for accretionary systems. J Geophys Res 95:8969–8982. https://doi.org/10.1029/JB095iB06p08969

Brown KM, Saffer DM, Bekins BA (2001) Smectite diagenesis, pore-water freshening, and fluid flow at the toe of the Nankai wedge. Earth Planet Sci Lett 194:97–109. https://doi.org/10.1016/S0012-821X(01)00546-5

Brunnegård J, Grandel S, Ståhl H, Tengberg A, Hall PO (2004) Nitrogen cycling in deep-sea sediments of the Porcupine Abyssal

Plain, NE Atlantic. Progr Oceanogr 63:159–181. https://doi.org/10.1016/j.pocean.2004.09.004
Burdige DJ, Komada T (2011) Anaerobic oxidation of methane and the stoichiometry of remineralization processes in continental margin sediments. Limnol Oceanogr 56:1781–1796. https://doi.org/10.4319/lo.2011.56.5.1781
Burgos M, Sierra A, Ortega T, Forja JM (2015) Anthropogenic effects on greenhouse gas (CH_4 and N_2O) emissions in the Guadalete River Estuary (SW Spain). Sci Total Enviro 503:179–189. https://doi.org/10.1016/j.scitotenv.2014.06.038
Cai WJ, Wiebe WJ, Wang Y, Sheldon JE (2000) Intertidal marsh as a source of dissolved inorganic carbon and a sink of nitrate in the Satilla River-estuarine complex in the southeastern U.S. Limnol Oceanogr 45:1743–1752. https://doi.org/10.4319/lo.2000.45.8.1743
Canfield D, Kristensen E, Thamdrup B (2005) Advances in marine biology. Aquatic Geomicrobiology, pp. 656
Carvalho L, Monteiro R, Figueira P, Mieiro C, Almeida J, Pereira E, Magalhães V, Pinheiro L, Vale C (2018) Vertical distribution of major, minor and trace elements in sediments from mud volcanoes of the Gulf of Cadiz: evidence of Cd, As and Ba fronts in upper layers. Deep Sea Res Part I: Oceanogr Res Pap 131:133–143. https://doi.org/10.1016/j.dsr.2017.12.003
Cermelj B, Bertuzzi A, Faganeli J (1997) Modelling of pore water nutrient distribution and benthic fluxes in shallow coastal waters (Gulf of Trieste, Northern Adriatic). In: Evans R.D., Wisniewski J., Wisniewski J.R. (eds) The Interactions Between Sediments and Water. Springer, Dordrecht, pp. 435–443. https://doi.org/10.1007/978-94-011-5552-6_45
Charlou JL, Donval JP, Zitter T, Roy N, Jean-Baptiste P, Foucher JP, Woodside J (2003) Evidence of methane venting and geochemistry of brines on mud volcanoes of the eastern Mediterranean Sea. Deep Sea Res Part I: Oceanogr Res Pap 50:941–958. https://doi.org/10.1016/S0967-0637(03)00093-1
Christensen JP, Murray JW, Devol AH, Codispoti LA (1987) Denitrification in continental shelf sediments has major impact on the oceanic nitrogen budget. Glob Biogeochem Cycles 1:97–116. https://doi.org/10.1029/GB001i002p00097
Coffin R, Hamdan L, Plummer R, Smith J, Gardner J, Hagen R, Wood W (2008) Analysis of methane and sulfate flux in methane-charged sediments from the Mississippi Canyon, Gulf of Mexico. Mar Pet Geol 25:977–987. https://doi.org/10.1016/j.marpetgeo.2008.01.014
Colten-Bradley VA (1987) Role of pressure in smectite dehydration-effects on geopressure and smectite-to-illite transformation. Am Assoc Petrol Geol Bull 71:1414–1427. https://doi.org/10.1306/703C8092-1707-11D7-8645000102C1865D
Dählmann A, de Lange GJ (2003) Fluid-sediment interactions at Eastern Mediterranean mud volcanoes: a stable isotope study from ODP Leg 160. Earth Planet Sci Lett 212:377–391. https://doi.org/10.1016/S0012-821X(03)00227-9
Denis L, Grenz C, Alliot E, Rodier M (2001) Temporal variability in dissolved inorganic nitrogen fluxes at the sediment-water interface and related annual budget on a continental shelf (NW Mediterranean). Oceanol Acta 24:85–97. https://doi.org/10.1016/S0399-1784(00)01130-0
Diaz-del-Rio V, Somoza L, Martinez-Frias J, Mata JP, Delgado A, Hernandez-Molina FJ, Lunar R, Martin-Rubi JA, Maestro A, Fernandez-Puga MC, Leon R, Llave E, Medialdea T, Vázquez JT (2003) Vast fields of hydrocarbon-derived carbonate chimneys related to the accretionary wedge/olistostrome of the Gulf of Cadiz. Mar Geol 195:177–200. https://doi.org/10.1016/S0025-3227(02)00687-4
Díaz-del-Río V, Bruque G, Fernández Salas LM, Rueda JL, González E, López N, Palomino D, López FJ, Farias C, Sánchez R, Vázquez JT, Rittierott CC, Fernández A, Marina P, Luque V, Oporto T, Sánchez O, García M, Urra J, Bárcenas P, Jiménez MP, Sagarminaga R, Arcos JM (2014) Volcanes de fango del golfo de Cádiz, Proyecto LIFE+ INDEMARES. Ed. Fundación Biodiversidad del Ministerio de Agricultura, Alimentación y Medio Ambiente, Madrid (España), pp. 128
Dickson AG (1990) Thermodynamics of the dissociation of boric acid in synthetic seawater from 273.15 to 318.15 K. Deep Sea Res Part A Oceanogr Res Pap 37:755–766. https://doi.org/10.1016/0198-0149(90)90004-F
Dimitrov LI (2002) Mud volcanoes-the most important pathway for degassing deeply buried sediments. Earth-Sci Rev 59:49–76. https://doi.org/10.1016/S0012-8252(02)00069-7
Dimitrov LI (2003) Mud volcanoes-a significant source of atmospheric methane. Geo-Mar Lett 23:155–161. https://doi.org/10.1007/s00367-003-0140-3
Dupré S, Berger L, Le Bouffant N, Scalabrin C, Bourillet J-F (2014) Fluid emissions at the Aquitaine Shelf (Bay of Biscay, France): a biogenic origin or the expression of hydrocarbon leakage? Cont Shelf Res 88:24–33. https://doi.org/10.1016/j.csr.2014.07.004
Egger M, Riedinger N, Mogollón JM, Jørgensen BB (2018) Global diffusive fluxes of methane in marine sediments. Nature Geosci 11:421–425. https://doi.org/10.1038/s41561-018-0122-8
Emerson S, Jahnke R, Bender M, Froelich P, Klinkhammer G, Bowser C, Setlock G (1980) Early diagenesis in sediments from the eastern equatorial Pacific, I. Pore water nutrient and carbonate results. Earth Planet Sci Lett 49:57–80. https://doi.org/10.1016/0012-821X(80)90150-8
Feng J, Yang SX, Liang JQ, Fang YX, He YL, Luo M, Chen DF (2018) Methane seepage inferred from the pore water geochemistry of shallow sediments in the Beikang Basin of the southern South China Sea. J Asian Earth Sci 168:77–86. https://doi.org/10.1016/j.jseaes.2018.02.005
Fernández-Puga MC (2004) Diapirismo y estructuras de expulsión de gases hidrocarburos en el talud continental del Golfo de Cádiz. PhD Thesis. Facultad de Ciencias del Mar, University of Cádiz, Spain, pp. 336
Fernández-Puga MC, Vázquez JT, Somoza L, Díaz del Rio V, Medialdea T, Mata MP, León R (2007) Gas-related morphologies and diapirism in the Gulf of Cádiz. Geo-Mar Lett 27:213–221. https://doi.org/10.1007/s00367-007-0076-0
Fernández-Salas LM, Sánchez Leal RF, Rueda JL, López-González N, González-García E, López-Rodríguez FJ, Bruque G, Vázquez JT, Díaz-del-Río V (2012) Interacción entre las masas de agua, los relieves submarinos y la distribución de especies bentónicas en el talud con- tinental del Golfo de Cádiz. Geo-Temas 13:198
Flint AL, Flint LE (2002) Particle Density. In: Dane, J.H., Topp, G.C. (eds) Methods of soil analysis. Part 4. Physical methods. Soil Science Society of America, Madison, Wisconsin, pp. 229–240. https://doi.org/10.2136/sssabookser5.4.c10
Froelich PN, Klinkhammer GP, Bender ML, Luedtke NA, Heath GR, Cullen D, Dauphin P, Hammond D, Hartman B, Maynard V (1979) Early oxidation of organic-matter in pelagic sediments of the eastern equatorial Atlantic-suboxic diagenesis. Geochim Cosmochim Acta 43:1075–1090. https://doi.org/10.1016/0016-7037(79)90095-4
Grasshoff K, Ehrhardt M (1983) Automated chemical analysis. Methods of Seawater Analysis. Verlag Chemie, Weinheim, pp 263–289
Grasshoff K, Ehrhardt M, Kremling K (1983) Methods of seawater analysis. Verlag Chemie, New York, pp. 419. https://doi.org/10.1002/iroh.19850700232
Haese RR, Meile C, Van Cappellen P, De Lange GJ (2003) Carbon geochemistry of cold seeps: methane fluxes and transformation in sediments from Kazan mud volcano, eastern Mediterranean Sea. Earth Planet Sci Lett 212:361–375. https://doi.org/10.1016/S0012-821X(03)00226-7

Haese RR, Hensen C, De Lange GJ (2006) Pore water geochemistry of eastern Mediterranean mud volcanoes: implications for fluid transport and fluid origin. Mar Geol 225:191–208. https://doi.org/10.1016/j.margeo.2005.09.001

Haffert L, Haeckel M, Liebetrau V, Berndt C, Hensen C, Nuzzo M, Reitz A, Scholz F, Schönfeld J, Perez-Garcia C, Weise SM (2013) Fluid evolution and authigenic mineral paragenesis related to salt diapirism - the Mercator mud volcano in the Gulf of Cadiz. Geochim Cosmochim Acta 106:261–286. https://doi.org/10.1016/j.gca.2012.12.016

Hedges JI, Stern JH (1984) Carbon and nitrogen determinations of carbonate-containing solids. Limnol Oceanogr 29:657–663. https://doi.org/10.4319/lo.1984.29.3.0657

Hensen C, Zabel M, Schulz HD (2000) A comparison of benthic nutrient fluxes from deep-sea sediments off Namibia and Argentina. Deep Sea Res Part II: Top Stud Oceanogr 47:2029–2050. https://doi.org/10.1016/S0967-0645(00)00015-1

Hensen C, Zabel M, Pfeifer K, Schwenk T, Kasten S, Riedinger N, Schulz HD, Boetius A (2003) Control of sulfate pore-water profiles by sedimentary events and the significance of anaerobic oxidation of methane for the burial of sulfur in marine sediments. Geochim Cosmochim Acta 67:2631–2647. https://doi.org/10.1016/S0016-7037(03)00199-6

Hensen C, Nuzzo M, Hornibrook E, Pinheiro LM, Bock B, Magalhães VH, Brückmann W (2007) Sources of mud volcano fluids in the Gulf of Cadiz-indications for hydrothermal imprint. Geochim Cosmochim Acta 71:1232–1248. https://doi.org/10.1016/j.gca.2006.11.022

Hensen C, Scholz F, Nuzzo M, Valadares V, Gràcia E, Terrinha P, Liebetrau V, Kaul N, Silva S, Martínez-Loriente S, Bartolome R, Piñero E, Magalhães VH, Schmidt M, Weise SM, Cunha M, Hilario A, Perea H, Rovelli L, Lackschewitz K (2015) Strike-slip faults mediate the rise of crustal-derived fluids and mud volcanism in the deep sea. Geology 43:339–342. https://doi.org/10.1130/G36359.1

Hower J, Eslinger EV, Hower ME, Perry EA (1976) Mechanism of burial metamorphism of argillaceous sediment: 1. Mineralogical and chemical evidence. Geol Soc Amer Bull 87:725–737. https://doi.org/10.1130/0016-7606(1976)87%3c725:MOBMOA%3e2.0.CO;2

Hu Y, Feng D, Liang Q, Xia Z, Chen L, Chen D (2015) Impact of anaerobic oxidation of methane on the geochemical cycle of redox-sensitive elements at cold-seep sites of the northern South China Sea. Deep Sea Res Part II: Top Stud Oceanogr 122:84–94. https://doi.org/10.1016/j.dsr2.2015.06.012

Hu CY, Frank Yang T, Burr GS, Chuang PC, Chen HW, Walia M, Chen NC, Huang YC, Lin S, Wang Y, Chung SH, Huang CDa Chen CH, (2017) Biogeochemical cycles at the sulfate-methane transition zone (SMTZ) and geochemical characteristics of the pore fluids offshore southwestern Taiwan. J Asian Earth Sci 149:172–183. https://doi.org/10.1016/j.jseaes.2017.07.002

Huguen C, Foucher JP, Mascle J, Ondréas H, Thouement M, Gontharet S, Stadnitskaia A, Pierre C, Bayon G, Loncke L, Boetius A, Bouloubassi I, de Lange G, Caprais JC, Fouquet Y, Woodside J, Dupré S (2009) Menes caldera, a highly active site of brine seepage in the Eastern Mediterranean sea: "in situ" observations from the NAUTINIL expedition (2003). Mar Geol 261:138–152. https://doi.org/10.1016/j.margeo.2009.02.005

Ivanov MK, Kenyon N, Nielsen T, Wheeler A, Monteiro H, Gardner J, Comas M, Akhmanov A, Akhmetzhanov G (2000) Goals and principal results of the TTR-9 cruise. IOC/UNESCO Work Rep 168:3–4

Iversen N, Jørgensen BB (1993) Diffusion coefficients of sulfate and methane in marine sediments: influence of porosity. Geochim Cosmo Acta 57:571–578. https://doi.org/10.1016/0016-7037(93)90368-7

Jayakumar DA, Naqvi SWA, Narvekar PV, George MD (2001) Methane in coastal and offshore waters of the Arabian Sea. Mar Chem 74:1–13. https://doi.org/10.1016/S0304-4203(00)00089-X

Jensen HS, Mortensen PB, Andersen FO, Rasmussen E, Jensen A (1995) Phosphorus cycling in a coastal marine sediment, Aarhus Bay, Denmark. Limnol Oceanogr 40:908–917. https://doi.org/10.4319/lo.1995.40.5.0908

Jørgensen BB, Revsbech NP (1989) Oxygen uptake, bacterial distribution, and carbon–nitrogen–sulfur cycling in sediments from the Baltic Sea-North Sea transition. Ophelia 31:29–49. https://doi.org/10.1080/00785326.1989.10430849

Judd A, Hovland M (2007) Seabed fluid flow: the impact on geology, biology, and the marine environment. Cambridge Univ. Press, pp. 475. https://doi.org/10.1017/CBO9780511535918

Judd A, Hovland M, Dimitrov LI, García Gil S, Jukes V (2002) The geological methane budget at continental margins and its influence on climate change. Geofluids 2:109–126. https://doi.org/10.1046/j.1468-8123.2002.00027.x

Kastner M, Elderfield H, Martin JB, Suess E, Kvenvolden KA, Garrison REDiagenesis and interstitial-water chemistry at the Peruvian continental margin—major constituents and strontium isotopes. In Suess, E., von Huene, R., et al (1990) Proc Ocean Drill Progr Sci Results 112:413–440

Kastner M, Claypool G, Robertson G (2008) Geochemical constraints on the origin of the pore fluids and gas hydrate distribution at Atwater Valley and Keathley Canyon, northern Gulf of Mexico. Mar Petrol Geol 25:860–872. https://doi.org/10.1016/j.marpetgeo.2008.01.022

Kim J-H, Torres ME, Hong W-L, Choi J, Bahk J-J, Kim S-H (2013) Pore fluid chemistry from the second gas hydrate drilling expedition in the Ulleung Basin (UBGH2) source mechanisms and consequences of fluid freshening in the central part of the Ulleung Basin East Sea. Mar Pet Geol 47:99–112. https://doi.org/10.1016/J.MARPETGEO.2012.12.011

Kopf AJ (2002) Significance of mud volcanism. Rev Geophys 40:2–46. https://doi.org/10.1029/2000RG000093

Kopf AJ (2003) Global methane emission through mud volcanoes and its past and present impact on the Earth's climate. Int J Earth Sci 92:806–816. https://doi.org/10.1007/s00531-003-0341-z

Krom MD, Berner RA (1980) Adsorption of phosphate in anoxic marine sediments 1. Limnol Oceanogr 25:797–806. https://doi.org/10.4319/lo.1980.25.5.0797

Krumins V, Gehlen M, Arndt S, Van Cappellen P, Regnier P (2013) Dissolved inorganic carbon and alkalinity fluxes from coastal marine sediments: model estimates for different shelf environments and sensitivity to global change. Biogeosciences 10:371–398. https://doi.org/10.5194/bg-10-371-2013

Lee K, Kim TW, Byrne RH, Millero FJ, Feely RA, Liu YM (2010) The universal ratio of boron to chlorinity for the North Pacific and North Atlantic oceans. Geochim Cosmochim Acta 74:1801–1811. https://doi.org/10.1016/j.gca.2009.12.027

Lee D-H, Kim J-H, Lee YM, Stadnitskaia A, Jin YK, Niemann H, Kim Y-G, Shin K-H (2018) Biogeochemical evidence of anaerobic methane oxidation on active submarine mud volcanoes on the continental slope of the Canadian Beaufort Sea. Biogeosciences 15:7419–7433. https://doi.org/10.5194/bg-15-7419-2018

León R, Somoza L, Medialdea T, Vázquez JT, González FJ, López-González N, Casas D, Mata MP, Fernández-Puga MC, Giménez-Moreno CJ, Díaz-del-Río V (2012) New discoveries of mud volcanoes on the Moroccan Atlantic continental margin (Gulf of Cádiz): morpho-structural characterization. Geo-Mar Lett 32:473–488. https://doi.org/10.1007/s00367-012-0275-1

Lewis E,Wallace DWR, Allison LJ (1998) Program developed for CO_2 system calculations. ORNL/CDIAC-105. Carbon Dioxide Information Analysis Center, Oak Ridge National Laboratory,

U.S. Department of Energy, Oak Ridge, Tennessee, pp. 42. https://doi.org/10.2172/639712
Li Y-H, Gregory S (1974) Diffusion of ions in sea water and in deep sea sediments. Geochim Cosmo Acta 38:703–714. https://doi.org/10.1016/0016-7037(74)90145-8
Li N, Huang H, Chen D (2014) Fluid sources and chemical processes inferred from geochemistry of pore fluids and sediments of mud volcanoes in the southern margin of the Junggar Basin, Xinjiang, northwestern China. Appl Geochem 46:1–9. https://doi.org/10.1016/j.apgeochem.2014.04.007
Lin S, Wei-Chi H, Lim YC, Yang TF, Liu CS, Wang Y (2006) Methane migration and its influence on sulfate reduction in the Good Weather Ridge region, South China Sea continental margin sediments. Terr Atmos Ocean Sci 17:883–902. https://doi.org/10.3319/TAO.2006.17.4.883(GH)
Loyd SJ, Berelson WM (2016) The modern record of "concretionary" carbonate: reassessing a discrepancy between modern sediments and the geologic record. Chem Geol 420:77–87. https://doi.org/10.1016/j.chemgeo.2015.11.009
Lozano P, Fernández-Salas LM, Hernández-Molina FJ, Sánchez-Leal R, Sánchez-Guillamón O, Palomino D, Farias C, Mateo-Ramírez A, López-González N, Vázquez J-T, Vila Y, Rueda JL (2020) Multiprocess interaction shaping geoforms and controlling substrate types and benthic community distribution in the Gul of Cádiz. Mar Geol 423:106139. https://doi.org/10.1016/j.margeo.2020.106139
Lueker TJ, Dickson AG, Keeling CD (2000) Ocean pCO_2 calculated from dissolved inorganic carbon, alkalinity, and equations for K_1 and K_2: validation based on laboratory measurements of CO_2 in gas and seawater at equilibrium. Mar Chem 70:105–119. https://doi.org/10.1016/S0304-4203(00)00022-0
Luo M, Chen L, Wang S, Yan W, Wang H, Chen D (2013) Pockmark activity inferred from pore water geochemistry in shallow sediments of the pockmark field in southwestern Xisha Uplift, northwestern South China Sea. Mar Petrol Geol 48:247–259. https://doi.org/10.1016/j.marpetgeo.2013.08.018
Magalhaes VH, Buffett B, Archer D, McGuire PC, Pinheiro LM, Gardner JM (2019) Effects of oceanographic changes on controlling the stability of gas hydrates and the formation of authigenic carbonates at mud volcanoes and seepage sites on the Iberian margin of the Gulf of Cadiz. Mar Geol 412:69–80. https://doi.org/10.1016/j.margeo.2019.03.002
Maldonado A, Somoza L, Pallarés L (1999) The Betic orogen and the Iberian-African boundary in the Gulf of Cádiz: geological evolution (central North Atlantic). Mar Geol 155:9–43. https://doi.org/10.1016/S0025-3227(98)00139-X
Martens CS, Berner RA (1974) Methane production in the interstitial waters of sulfate-depleted marine sediments. Science 185:1167–1169. https://doi.org/10.1126/science.185.4157.1167
Martin JB, Kastner M, Henry P, Le Pichon X, Lallement S (1996) Chemical and isotopic evidence for sources of fluids in a mud volcano field seaward of the Barbados accretionary wedge. J Geophys Res 101:20325–20345. https://doi.org/10.1029/96JB00140
Martos-Villa R, Mata MP, Williams LB, Nieto F, Arroyo Rey X, Sainz-Díaz CI (2020) Evidence of hydrocarbon-rich fluid interaction with clays: clay mineralogy and boron isotope data from Gulf of Cádiz mud volcano sediments. Minerals 10:651. https://doi.org/10.3390/min10080651
Mazurenko LL, Soloviev VA, Belenkaya I, Ivanov MK, Pinheiro LM (2002) Mud volcano gas hydrates in the Gulf of Cadiz. Terra Nov 14:321–329. https://doi.org/10.1046/j.1365-3121.2002.00428.x
Medialdea T, Vegas R, Somoza L, Vázquez JT, Maldonado A, Díaz-Del-Río V, Maestro A, Córdoba D, Fernández-Puga MC (2004) Structure and evolution of the "Olistostrome" complex of the Gibraltar Arc in the Gulf of Cádiz (eastern Central Atlantic): evidence from two long seismic cross-sections. Mar Geol 209:173–198. https://doi.org/10.1016/j.margeo.2004.05.029
Medialdea T, Somoza L, Pinheiro LM, Fernández-Puga MC, Vázquez JT, León R, Ivanov MK, Magalhaes V, Díaz-del-Río V, Vegas R (2009) Tectonics and mud volcano development in the Gulf of Cádiz. Mar Geol 261:48–63. https://doi.org/10.1016/j.margeo.2008.10.007
Milkov AV (2000) Worldwide distribution of submarine mud volcanoes and associated gas hydrates. Mar Geol 167:29–42. https://doi.org/10.1016/S0025-3227(00)00022-0
Milkov AV, Etiope G (2005) Global methane emission through mud volcanoes and its past and present impact on the Earth's climate-a comment. Int J Earth Sci 94:490–492. https://doi.org/10.1007/s00531-005-0480-5
Milkov AV, Sassen R, Apanasovich TV, Dadashev FG (2003) Global gas flux from mud volcanoes: a significant source of fossil methane in the atmosphere and the ocean. Geophys Res Lett 30:17–20. https://doi.org/10.1029/2002GL016358
Millero FJ (2013) Chemical oceanography. CRC press, pp. 591
Moore TS, Murray RW, Kurtz AC, Schrag DP (2004) Anaerobic methane oxidation and the formation of dolomite. Earth Planet Sci Lett 229:141–154. https://doi.org/10.1016/j.epsl.2004.10.015
Mucci A, Sundby B, Gehlen M, Arakaki T, Zhong S, Silverberg N (2000) The fate of carbon in continental shelf sediments of eastern Canada: a case study. Deep Sea Res Part II: Top Stud Oceanogr 47:733–760. https://doi.org/10.1016/S0967-0645(99)00124-1
Munsell Color Chart (2000) Munsell soil color charts revised, washable. New Windsor, New York, Gretabacbeth, Munsell Color
Nakada R, Takahashi Y, Tsunogai U, Zheng G, Shimizu H, Hattori KH (2011) A geochemical study on mud volcanoes in the Junggar Basin, China. Appl Geochem 26:1065–1076. https://doi.org/10.1016/j.apgeochem.2011.03.011
Niemann H (2020) Mud volcano biogeochemistry. In: Wilkes H. (eds) Hydrocarbons, oils and lipids: diversity, origin, chemistry and fate. Handbook of Hydrocarbon and Lipid Microbiology. Springer, Cham. https://doi.org/10.1007/978-3-319-54529-5_28-1
Niemann H, Duarte J, Hensen C, Omoregie E, Magalhães VH, Elvert M, Pinheiro LM, Kopf A, Boetius A (2006) Microbial methane turnover at mud volcanoes of the Gulf of Cadiz. Geochim Cosmochim Acta 70:5336–5355. https://doi.org/10.1016/j.gca.2006.08.010
Nuzzo M, Hornibrook ERC, Hensen C, Parkes RJ, Cragg BA, Rinna J, Schneider von Deimling J, Sommer S, Magalhães VH, Reitz A, Brückmann W, Pinheiro LM (2008) Shallow microbial recycling of deep-sourced carbon in Gulf of Cadiz mud volcanoes. Geomicrobiol J 25:283–295. https://doi.org/10.1080/01490450802258196
Nuzzo M, Hornibrook ERC, Gill F, Hensen C, Pancost RD, Haeckel M, Reitz A, Scholz F, Magalhães VH, Brückmann W, Pinheiro LM (2009) Origin of light volatile hydrocarbon gases in mud volcano fluids, Gulf of Cadiz - evidence for multiple sources and transport mechanisms in active sedimentary wedges. Chem Geol 266:350–363. https://doi.org/10.1016/j.chemgeo.2009.06.023
Orphan VJ, House CH, Hinrichs KU, McKeegan KD, DeLong EF (2001) Methane- consuming archaea revealed by directly coupled isotopic and phylogenetic analysis. Science 293:484–487. https://doi.org/10.1126/science.1061338
Ortega T, Ponce R, Forja J, Gómez-Parra A (2008) Benthic fluxes of dissolved inorganic carbon in the Tinto-Odiel system (SW of Spain). Cont Shelf Res 28:458–469. https://doi.org/10.1016/j.csr.2007.10.004
Palomino D, López-González N, Vázquez J-T, Fernández-Salas L-M, Rueda J-L, Sánchez-Leal R, Díaz-del-Río V (2016) Multidisciplinary study of mud volcanoes and diapirs and their relationship to seepages and bottom currents in the Gulf of Cádiz continental

slope (northeastern sector). Mar Geol 378:196–212. https://doi.org/10.1016/j.margeo.2015.10.001

Peckmann J, Reimer A, Luth U, Luth C, Hansen BT, Heinicke C, Hoefs J, Reitner J (2001) Methane-derived carbonates and authigenic pyrite from the northwestern Black Sea. Mar Geol 177:129–150. https://doi.org/10.1016/S0025-3227(01)00128-1

Pereira E, Vale C, Monteiro R, Pinheiro L, Carvalho L, Magalhães V, Figueira P, Mieiro C (2018) Rare earth elements in mud volcano sediments from the Gulf of Cadiz, South Iberian Peninsula. Sci Total Environ 652:869–879. https://doi.org/10.1016/j.scitotenv.2018.10.227

Perry ED, Hower J (1970) Burial diagenesis in Gulf Coast Pelitic Sediments. Clays Clay Miner 18:165–177. https://doi.org/10.1346/CCMN.1970.0180306

Pierre C, Blanc-Valleron M-M, Demange J, Boudouma O, Foucher J-P, Pape T, Himmler T, Fekete N, Spiess V (2012) Authigenic carbonates from active methane seeps off shore southwest Africa. Geo-Mar Lett 32:501–513. https://doi.org/10.1007/s00367-012-0295-x

Pinheiro LM, Ivanov MK, Sautkin A, Akhmanov G, Magalhães VH, Volkonskaya A, Monteiro JH, Somoza L, Gardner J, Hamouni N, Cunha MR (2003) Mud volcanism in the Gulf of Cadiz: results from the TTR-10 cruise. Mar Geol 195:131–151. https://doi.org/10.1016/S0025-3227(02)00685-0

Rabouille C, Gaillard J-F (1991) A model representing the deep sea organic carbon mineralization and oxygen consumption in surficial sediments. J Geophys Res 96:2761–2776. https://doi.org/10.1029/90JC02332

Reeburgh WS (2007) Oceanic methane biogeochemistry. Chem Rev 107:486–513. https://doi.org/10.1021/cr050362v

Reitz A, Haeckel M, Wallmann K, Hensen C, Heeschen K (2007) Origin of salt-enriched pore fluids in the northern Gulf of Mexico. Earth Planet Sci Lett 259:266–282. https://doi.org/10.1016/j.epsl.2007.04.037

Ritger S, Carson B, Suess E (1987) Methane-derived authigenic carbonates formed by subduction-induced pore-water expulsion along the Oregon/Washington margin. Geol Soc Amer Bull 98:147–156. https://doi.org/10.1130/0016-7606(1987)98%3c147:MACFBS%3e2.0.CO;2

Rodrigues CF, Hilário A, Cunha MR (2013) Chemosymbiotic species from the Gulf of Cadiz (NE Atlantic): distribution, life styles and nutritional patterns. Biogeosciences 10:2569–2581. https://doi.org/10.5194/bg-10-2569-2013

Rosas FM, Duarte JC, Neves MC, Terrinha P, Silva S, Matias L, Gràcia E, Bartolome R (2012) Thrust–wrench interference between major active faults in the Gulf of Cadiz (Africa–Eurasia plate boundary, offshore SW Iberia): tectonic implications from coupled analog and numerical modeling. Tectonophysics 548:1–21. https://doi.org/10.1016/j.tecto.2012.04.013

Rueda JL, Urra J, Gofas S, López-González N, Fernández-Salas LM, Díaz-del-Río V (2012) New records of recently described chemosymbiotic bivalves for mud volcanoes within the European waters (Gulf of Cádiz). Mediterr Mar Sci 13:262–267. https://doi.org/10.12681/mms.307

Rueda JL, González-García E, Krutzky C, López-Rodriguez FJ, Bruque G, López-González N, Palomino D, Sánchez RF, Vázquez JT, Fernández-Salas LM, Díaz-del-Río V (2016) From chemosynthesis-based communities to cold-water corals: vulnerable deep-sea habitats of the Gulf of Cádiz. Mar Biodiver 46:473–482. https://doi.org/10.1007/s12526-015-0366-0

Sánchez-Guillamón O (2019) Deep submarine volcanoes in two different settings (Canary basin and Gulf of Cádiz): morphology and shallow structure. PhD Thesis. pp. 303

Sarmiento JL, Gruber N (2004) Remineralization and burial in the sediments. Ocean biogeochemical dynamics. Princeton University Press, Princeton, New Jersey, USA, pp 227–267

Sasaki KI, Noriki S, Tsunogai S (2001) Vertical distributions of interstitial phosphate and fluoride in anoxic sediment: insight into the formation of an authigenic fluorophosphorus compound. Geochem J 35:295–306. https://doi.org/10.2343/geochemj.35.295

Schmidt C, Burwicz E, Hensen C, Wallmann K, Martínez-Loriente S, Gràcia E (2018) Genesis of mud volcano fluids in the Gulf of Cadiz using a novel basin-scale model approach. Geochim Cosmochim Acta 243:186–204. https://doi.org/10.1016/j.gca.2018.09.011

Scholz F, Hensen C, Reitz A, Romer RL, Liebetrau V, Meixner A, Weise SM, Haeckel M (2009) Isotopic evidence ($^{87}Sr/^{86}Sr$, $\delta^{7}Li$) for alteration of the oceanic crust at deep-rooted mud volcanoes in the Gulf of Cadiz, NE Atlantic Ocean. Geochim Cosmochim Acta 73:5444–5459. https://doi.org/10.1016/j.gca.2009.06.004

Schuffert JD, Kastner M, Jahnke RA (1998) Carbon and phosphorus burial associated with modern phosphorite formation. Mar Geol 146:21–31. https://doi.org/10.1016/S0025-3227(97)00122-9

Schulz HD (2006) Conceptual models and computer models. In: Schulz, H.D., Zabel, M. (eds) Marine Geochemistry, 2. Edn. Springer-Verlag, Berlin, Heidelberg, New York, pp. 513–547. https://doi.org/10.1007/3-540-32144-6_15

Sibuet M, Olu K (1998) Biogeography, biodiversity and fluid dependence of deep-sea cold-seep communities at active and passive margins. Deep Sea Res Part II: Top Stud Oceanogr 45:517–567. https://doi.org/10.1016/S0967-0645(97)00074-X

Sierra A, Jiménez-López D, Ortega T, Ponce R, Bellanco MJ, Sánchez-Leal R, Gómez-Parra A, Forja J (2017) Spatial and seasonal variability of CH_4 in the eastern Gulf of Cadiz (SW Iberian Peninsula). Sci Total Environ 590:695–707. https://doi.org/10.1016/j.scitotenv.2017.03.030

Sierra A, Jiménez-López D, Ortega T, Fernández-Puga MC, Delgado-Huertas A, Forja J (2020) Methane dynamics in the coastal–continental shelf transition zone of the Gulf of Cadiz. Estuar Coast Shelf Sci 236:106653. https://doi.org/10.1016/j.ecss.2020.106653

Soetaert K, Herman PMJ, Middelburg JJ (1996) A model for early diagenetic pro- cesses from the shelf to abyssal depths. Geochim Cosmochim Acta 60:1019–1040. https://doi.org/10.1016/0016-7037(96)00013-0

Sommer S, Türk M, Kriwanek S, Pfannkuche O (2008) Gas exchange system for extended in situ benthic chamber flux measurements under controlled oxygen conditions: first application - sea bed methane emission measurements at Captain Arutyunov mud volcano. Limnol Oceanogr Meth 6:23–33. https://doi.org/10.4319/lom.2008.6.23

Sommer S, Linke P, Pfannkuche O, Schleicher T, Schneider V, Deimling J, Reitz A, Haeckel M, Flögel S, Hensen C (2009) Seabed methane emissions and the habitat of frenulate tubeworms on the Captain Arutyunov mud volcano (Gulf of Cadiz). Mar Ecol Prog Ser 382:69–86. https://doi.org/10.3354/meps07956

Somoza L, Díaz-del-Río V, León R, Ivanov M, Fernández-Puga MC, Gardner JM, Hernández-Molina FJ, Pinheiro LM, Rodero J, Lobato A, Maestro A, Vázquez JT, Medialdea T, Fernández-Salas LM (2003) Seabed morphology and hydrocarbon seepage in the Gulf of Cádiz mud volcano area: acoustic imagery, multibeam and ultra-high resolution seismic data. Mar Geol 195:153–176. https://doi.org/10.1016/S0025-3227(02)00686-2

Srodon J (1999) Nature of mixed-layer clays and mechanisms of their formation and alteration. Annual Rev Earth Planet Sci 27:19–53. https://doi.org/10.1146/annurev.earth.27.1.19

Stadnitskaia A, Ivanov MK, Blinova V, Kreulen R, van Weering TCE (2006) Molecular and carbon isotopic variability of hydrocarbon gases from mud volcanoes in the Gulf of Cadiz, NE Atlantic. Mar Pet Geol 23:281–296. https://doi.org/10.1016/j.marpetgeo.2005.11.001

Terrinha P, Matias L, Vicente J, Duarte J, Luís J, Pinheiro L, Lourenço N, Diez S, Rosas F, Magalhães V, Valadares V, Zitellini N, Roque C, Mendez Víctor L MATESPRO Team (2009) Morphotectonics and strain partitioning at the Iberia-Africa plate boundary from multibeam and seismic reflection data. Mar Geol 267:156–174. https://doi.org/10.1016/j.margeo.2009.09.012

Trimmer M, Nicholls JC (2009) Production of nitrogen gas via anammox and denitrification in intact sediment cores along a continental shelf to slope transect in the North Atlantic. Limnol Oceanogr 54:577–589. https://doi.org/10.4319/lo.2009.54.2.0577

Udden JA (1914) Mechanical composition of clastic sediments. Geol Soc Amer Bull 25:655–744. https://doi.org/10.1130/GSAB-25-655

Usui T, Koike I, Ogura N (1998) Vertical profiles of nitrous oxide and dissolved oxygen in marine sediments. Mar Chem 59:253–270. https://doi.org/10.1016/S0304-4203(97)00091-1

Vanneste H, Kelly-Gerreyn BA, Connelly DP, James RH, Haeckel M, Fisher RE, Heeschen K, Mills RA (2011) Spatial variation in fluid flow and geochemical fluxes across the sediment-seawater interface at the Carlos Ribeiro mud volcano (Gulf of Cadiz). Geochim Cosmochim Acta 75:1124–1144. https://doi.org/10.1016/j.gca.2010.11.017

Vasconcelos C, McKenzie JA, Bernasconi S, Grujic D, Tien AJ (1995) Microbial mediation as a possible mechanism for natural dolomite formation at low temperatures. Nature 377:220–222. https://doi.org/10.1038/377220a0

Vázquez JT, Ercilla G, Catalán M, Do Couto D, Estrada F, Galindo-Zaldívar J, Juan C, Palomino D, Vegas R, Alonso B, Chalouan A, Ammar A, Azzouz O, Benmakhlouf M, d'Acremont E, Gorini C, Martos Y, Sanz de Galdeano C (2020) A geological history for the Alboran Sea region. In: Baéz, J.C., Camiñas, J.A., Vázquez, J.T., Malouli, M., (eds) Alboran sea and its marine resources. Springer Nature, Switzerland, AG. In press.

Wallmann K, Drews M, Aloisi G, Bohrmann G (2006) Methane discharge into the Black Sea and the global ocean via fluid flow through submarine mud volcanoes. Earth Planet Sci Lett 248:545–560. https://doi.org/10.1016/j.epsl.2006.06.026

Warthmann R, van Lith Y, Vasconcelos C, McKenzie JA, Karpoff A (2000) Bacterially induced dolomite precipitation in anoxic culture experiments. Geology 28:1091–1094. https://doi.org/10.1130/0091-7613(2000)28%3c1091:BIDPIA%3e2.0.CO;2

Weber T, Wiseman NA, Kock A (2019) Global ocean methane emissions dominated by shallow coastal waters. Nat Commun 10:1–10. https://doi.org/10.1038/s41467-019-12541-7

Wehrmann LM, Risgaard-Petersen N, Schrum HN, Walsh EA, Huh Y, Ikehara M, Pierre C, D'Hondt S, Ferdelman TG, Ravelo AC, Takahashi K, Zarikian CA (2011) Coupled organic and inorganic carbon cycling in the deep subseafloor sediment of the northeastern Bering Sea Slope (IODP Exp. 323). The Integrated Ocean Drilling Program Expedition 323 Scientific Party. Chem Geol 284:251–261. https://doi.org/10.1016/j.chemgeo.2011.03.002

Weiss RF, Price BA (1980) Nitrous oxide solubility in water and seawater. Mar Chem 8:347–359. https://doi.org/10.1016/0304-4203(80)90024-9

Wentworth CK (1922) A scale of grade and class terms for clastic sediments. J Geol 30:377–392

Wiesenburg DA, Guinasso NL Jr (1979) Equilibrium solubilities of methane, carbon monoxide, and hydrogen in water and sea water. J Chem Eng Data 24:356–360. https://doi.org/10.1021/je60083a006

Xu C, Wu N, Sun Z, Zhang X, Geng W, Cao H, Wang L, Zhang X, Xu G (2018) Methane seepage inferred from pore water geochemistry in shallow sediments in the western slope of the Mid-Okinawa Trough. Mar Pet Geol 98:306–315. https://doi.org/10.1016/j.marpetgeo.2018.08.021

Zeebe RE, Wolf-Gladrow D (2001) CO_2 in seawater: equilibrium, kinetics, isotopes. Elsevier Science, B.V, Elsevier, Amsterdam, p 346